Palaeogeography, Palaeoclimatology, Palaeoecology 536 (2019) 109395

Contents lists available at ScienceDirect

Palaeogeography, Palaeoclimatology, Palaeoecology

journal homepage: www.elsevier.com/locate/palaeo

# Integrated stratigraphy of the Eocene-Oligocene deposits of the northern Caucasus (Belaya River, Russia): Intermittent oxygen-depleted episodes in the Peri-Tethys and Paratethys

A. van der Boon[a,*], R. van der Ploeg[b], M.J. Cramwinckel[b], K.F. Kuiper[c], S.V. Popov[d], I.P. Tabachnikova[e], D.V. Palcu[a], W. Krijgsman[a]

[a] Paleomagnetic Laboratory 'Fort Hoofddijk', Utrecht University, the Netherlands, Budapestlaan 17, Utrecht
[b] Marine Palynology and Palaeoceanography, Department of Earth Sciences, Faculty of Geoscience, Utrecht University, Princetonlaan 8a, 3584, CB Utrecht, the Netherlands
[c] Dept. of Earth Sciences, Faculty of Science, Vrije Universiteit Amsterdam, De Boelelaan 1085, 1081HV, Amsterdam, the Netherlands
[d] Borrisiak Paleontological Institute, Russian Academy of Sciences, Ul. Profsoyuznaya 123, Moscow, 117647, Russia
[e] Karpinsky Russian Research Geological Institute (VSEGEI), Sredny pr. 74, St. Petersburg, 199106, Russia

ARTICLE INFO

*Keywords:*
Middle Eocene Climatic Optimum
MECO
Eocene-Oligocene Transition
Anoxia
Maikop
Kuma Formation

ABSTRACT

The sedimentary succession along the Belaya River (North Caucasus) provides a record of middle Eocene to Miocene sediments. This time interval is well known for its important climatic transitions (e.g., Middle Eocene Climate Optimum (MECO) and Eocene-Oligocene Transition (EOT)), and changes in basin configuration from Peri-Tethys to Paratethys. The Belaya section contains two intervals marked by oxygen-depleted sediments; the Eocene Kuma Formation of the Peri-Tethys and the Oligocene Maikop Group of the Paratethys. Both are considered important source rocks for hydrocarbon exploration in the Black Sea and Caspian Sea. We present integrated stratigraphic results of the Belaya River section using calcareous nannoplankton biostratigraphy, magnetostratigraphy and $^{40}Ar/^{39}Ar$ dating. Furthermore, we investigate the geochemical character of the sediments using X-ray fluorescence (XRF) and stable carbon and oxygen isotopes. A middle Eocene age for the lower part of the succession is established from nannoplankton biostratigraphy. The Kuma Formation is dated between 42.1 and 38.4 Ma based on the assumption of constant sediment accumulation rates. A negative oxygen isotope excursion in the middle part of the Kuma Formation could be related to the MECO (~40 Ma). The onset of the Maikop Group is dated around the base of chron C13n at an age of ~33.7 Ma, close to the Eocene-Oligocene boundary. Based on geochemical results, we show that the Kuma Formation and Maikop Group correspond to two different episodes of intensified oceanic oxygen depletion in the succession. We hypothesise that oxygen-depletion as recorded in the Kuma Formation is linked to an increased nutrient input in the open marine Peri-Tethys due to widespread volcanism in the Neotethys subduction zone, while oxygen-depletion as recorded in the Maikop Group is linked to basin restriction caused by the eustatic sea-level fall straddling the Eocene – Oligocene boundary triggering stratified conditions in the semi-isolated Paratethys Sea.

## 1. Introduction

The northern Caucasus has been the subject of hydrocarbon exploration for over 100 years, and has been extensively studied (Ershov et al., 2003, 1999; Grossheim, 1960; Prokopov, 1937), although most data are available only in Russian. The organic-rich shales of the Eocene Kuma Formation form a potential hydrocarbon source rock in this region, as they have a high TOC content (around 4% in the Belaya section; Sachsenhofer et al., 2018). The Kuma Formation is much smaller in stratigraphic thickness and regional volume compared to the Maikop Group, and remains less studied. Despite its relatively low hydrocarbon potential (Saint-Germes et al., 2000; Johnson et al., 2010; Sachsenhofer et al., 2017), the Oligo-Miocene Maikop Group is considered one of the most important source rocks in the former Paratethys (Guliyev et al., 2001; Hudson et al., 2008; Sachsenhofer and Schulz, 2006). In the Belaya section, the TOC content of the Maikop Group is around 1%

* Corresponding author. Geomagnetic Laboratory, Oliver Lodge Building, Department of Physics, Oxford Street, Liverpool, L69 7ZE, United Kingdom.
*E-mail addresses:* AvanderBoon.work@gmail.com (A. van der Boon), R.vanderPloeg@uu.nl (R. van der Ploeg), M.J.Cramwinckel@uu.nl (M.J. Cramwinckel), K.F.Kuiper@vu.nl (K.F. Kuiper), Serg.Pop@mail.ru (S.V. Popov), Irina_Tabachnikova@vsegei.ru (I.P. Tabachnikova), W.Krijgsman@uu.nl (W. Krijgsman).

https://doi.org/10.1016/j.palaeo.2019.109395
Received 5 March 2019; Received in revised form 1 October 2019; Accepted 1 October 2019
Available online 16 October 2019
0031-0182/ 

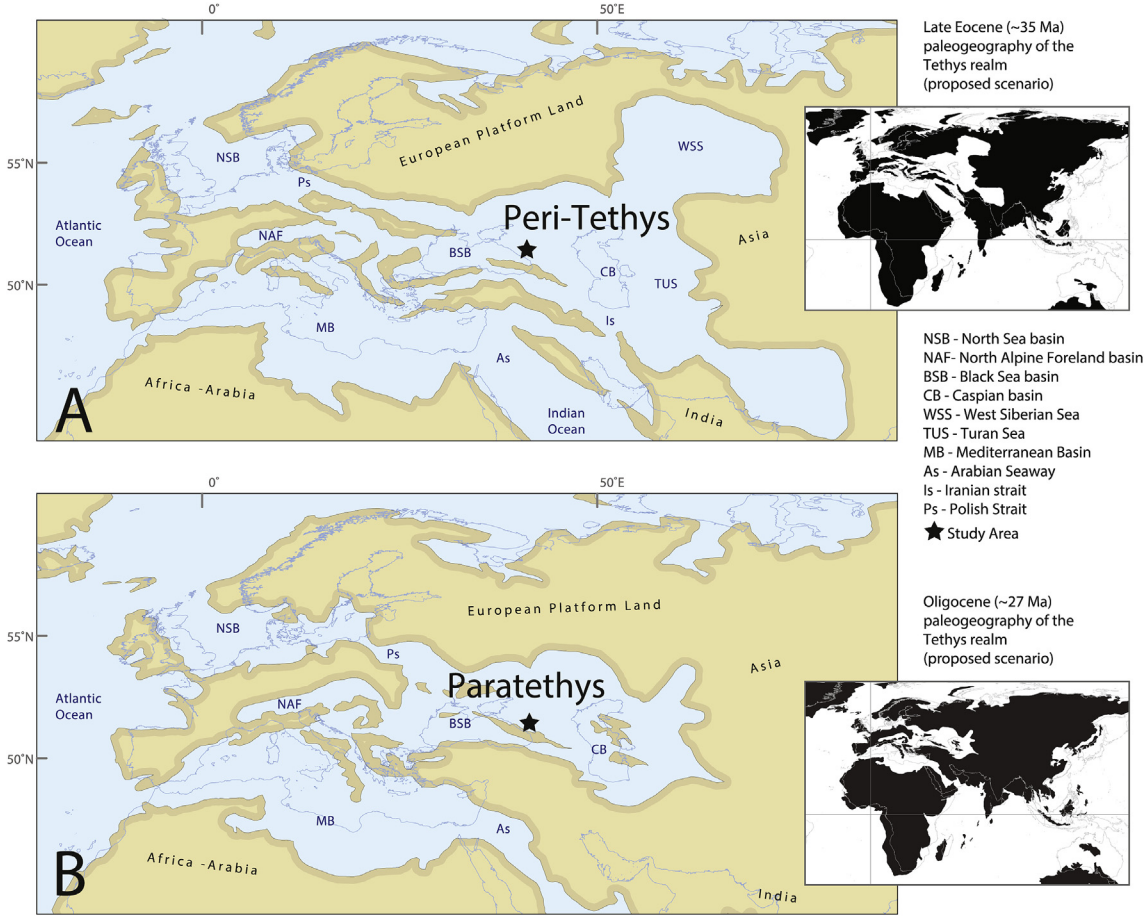


**Fig. 1.** Paleogeographic maps showing the differences in basin configuration from the late Eocene (~35 Ma) Peri-Tethys to the Oligocene Paratethys (~27 Ma).

(Sachsenhofer et al., 2018). Besides a hydrocarbon source rock, the Maikop Group is an important host of manganese ores (Stolyarov, 1993; Varentsov, 2002; Varentsov et al., 2003).

During the Eocene, the North Caucasus region was part of the Peri-Tethys domain, an open marine basin that covered large parts of central and eastern Europe and central Asia (see Fig. 1A). The Peri-Tethys was well-connected to the North Sea in the west, the Arctic ocean in the north (via the Turgay Strait before the Bartonian) and the Indian Ocean in the south (Popov et al., 2004a; Rögl, 1998). The Peri-Tethys transformed into the Paratethys around the Oligocene, as the basin became isolated (see Fig. 1) (e.g. Akhmetiev et al., 2012). Laskarev (1924) coined the term Paratethys, originally describing the environment of middle Miocene strata that contained endemic fossils. Later on, the definition was extended to include the Oligocene strata, which show the first isolation from the Mediterranean Sea and world oceans during the Solenovian (a regional Paratethys stage, covering part of the late Rupelian, see also Sachsenhofer et al. (2017))(Piller et al., 2004).

The Eocene Kuma Formation of the Peri-Tethys and the Oligocene Maikop Group of the Paratethys are both interpreted to have been deposited in low oxygen conditions in epicontinental basins (e.g. Beniamovski et al., 2003; Sachsenhofer et al., 2017). Lithological transitions from bioturbated light coloured carbonate sediments (limestone and marlstone) to dark organic-rich shales are described all over Central Eurasia, from the North Alpine foreland basin in the west (e.g. Bachmann and Müller, 1992) to the Caucasus (e.g. Shcherbinina and Gavrilov, 2007), South Aral area and Fore-Kopet Dagh in the east. The white marlstones are interpreted to have been deposited in well-oxygenated environments with abundant benthic fauna, while the organic-rich shales are linked to poorly ventilated bottom waters, strong water-column stratification and decreased connectivity to the open ocean (Schulz et al., 2005). The exact forcing mechanisms for oxygen depletion in the Peri-Tethys and Paratethys seas are still unclear.

Accurate dating of the onset and end of oxygen depletion could provide clues about causal processes and may help unravel climatic from geodynamic mechanisms (e.g. Palcu et al., 2019). If the onset of low oxygen conditions coincided with major climatic changes like the Eocene-Oligocene transition (EOT) and/or middle Eocene climatic optimum (MECO), the concomitant sea-level changes might have led to restricted conditions in the Peri-Tethys/Paratethys basins. Eustatic sea-level changes for the EOT are well-documented, but less constrained for the MECO (e.g. Dawber et al., 2011; Miller et al., 2009). However, Giorgioni et al. (2019) suggested that the MECO is related to major oceanographic changes in the Neotethys region and other basins. The Eocene-Oligocene transition is a time period of nearly half a million years, in which global climate changes in three steps that are characterised by isotope shifts; EOT-1, EOT-2 and Oi-1 (Houben et al., 2012). The Eocene-Oligocene boundary (EOB) is defined by the extinction of the hantkeninid planktonic foraminifera, and currently has an age of 33.9 Ma (Vandenberghe et al., 2012). EOT-1 is placed below the Eocene-Oligocene boundary, while EOT-2 and Oi-1 are placed above the EOB. The sea-level drop associated with Oi-1 is largest, with an estimated 50–60 m. Sea-level changes for EOT-1 are estimated at 20 m, while they are unconstrained for EOT-2 (Houben et al., 2012). Jovane et al. (2009) mentioned that the EOT is associated with large changes in circulation in the Neotethys region.

Alternatively, the Arabia-Eurasia continental collision might have played a role, by building topography, which could have restricted exchange between the Peri-Tethys/Paratethys and the open ocean. Timing of the Arabia-Eurasia collision is poorly constrained, with estimates ranging between 35 and 20 Ma (McQuarrie and van Hinsbergen,

2013). Furthermore, extensive volcanism related to subduction in the Neotethys (Iran-Azerbaijan) could have significantly increased nutrient fluxes to the basin, which could have induced low oxygen conditions through increasing surface ocean primary productivity coupled to increasing organic matter remineralisation in the water column (e.g. Adams et al., 2010). Although significant progress has been made during the last decades (e.g. Popov et al., 2004a,b, 2018; Benyamovskiy, 2012), a unified chronostratigraphy of the Eocene-Oligocene strata of the Peri-Tethys/Paratethys region is poorly constrained.

We perform integrated stratigraphy using calcareous nannofossil biostratigraphy, magnetostratigraphy and Ar–Ar dating to better constrain the ages of the Kuma Formation and the lower boundary of the Maikop Group. Additionally, we apply X-ray fluorescence (XRF) and stable carbon and oxygen isotope analyses to better understand the forcing mechanisms of low oxygen conditions that led to deposition of organic-rich shales in the Peri-Tethys and Paratethys.

## 2. Geologic setting

The type-locality of the Maikop Group is located in the North Caucasus, ~25 km south of Maikop, along the Belaya River (Republic of Adygea, Russia; see Fig. 2). The Belaya River section contains a well-exposed succession of Eocene-Oligocene strata and is interpreted to be continuous up to the mid-Rupelian (~30 Ma), after which the succession continues up into the Miocene with several gaps (Popov et al., 2019a).

The lowermost exposure consists of green mudstones of the Cherkessk Formation (e.g. Zakrevskaya et al., 2011), cropping out around 44.3665°N, 40.1970°E. These green mudstones are overlain by the Keresta Formation, consisting of white clayey marlstones (e.g. Benyamovskiy, 2012) that gradually transition to laminated, coffee-coloured marlstones of the Kuma Formation. The Kuma Formation contains sparse small pyrite nodules at the base, and abundant large ones (up to tens of centimetres Ø) at the top, near the transition to the Belaya Glina Formation. The Kuma Formation is characterized by high (> 0.5 wt%; Seiter et al., 2004) organic carbon contents (Sachsenhofer et al., 2018), abundant fish remains (bones and teeth) and wood fragments, and is mostly laminated. The top of the Kuma Formation appears to record cyclic alternations in lithology, visibly defined by differences in induration and colour. Typical cycle thickness around the Kuma-Belaya Glina boundary is 20–30 cm (see Fig. 3). The Belaya Glina Formation consists of white marlstones with abundant foraminifera and extensive bioturbation, and cyclic sedimentation is apparent throughout the entire formation. For a more detailed description of these formations in the Belaya section, we refer to Popov et al. (2019b).

The transition to the Pshekha Formation forms a sharp and conformable boundary. The Pshekha Formation, the oldest formation of the Maikop Group, consists of dark brown to black mudstones with abundant fish remains and overlies the Belaya Glina Formation. Just above the boundary with the Belaya Glina, the Pshekha Formation is represented by laminated mudstones containing Pteropoda (*Vaginella, Limacina*). The middle part of the formation contains a volcanic ash layer that is distinct in colour and contains visible biotite. Above the ash layer, there is a gap (estimated ~6 m, using bedding and Google Earth) in the section related to a curve in the river (Fig. 2). Downstream, the Pshekha Formation continues up to the Polbian bed. The Polbian bed is a calcareous nannoplankton-marlstone, and stands out as a distinctive white layer in the otherwise black Maikop Group. Polbian fauna indicates endemic and brackish affinities (e.g. Popov and Studencka, 2015 and references therein) and is recognized in the Central and Eastern Paratethys (Veto, 1987; Nagymarosy and Voronina, 1993). The Polbian bed is overlain by the Morozkina Balka Formation, which is interpreted to have high hydrocarbon potential (Sachsenhofer et al., 2017). The Lower Morozkina Balka subformation consists of dark, non-calcareous mudstones with fish remains. It contains five non-exposed intervals, of which thicknesses are estimated based on bedding orientation (the largest gap corresponds to ~9 m of stratigraphy missing). The Lower Morozkina Balka subformation is overlain by the Upper Morozkina Balka subformation, which contains thin calcareous sublayers (pellets) formed by nannofossils, and carbonate nodules. Younger formations of the Maikop Group (Batalpashinsk, Septarian, Karadzhalga, Olginskaya and Ritsa Formations; Sachsenhofer et al., 2017) crop out further downstream along the Belaya River. Beds are tilted slightly northwards, with a dip of 7–10°. Around the Belaya Glina-Pshekha transition, the dip is somewhat steeper (~20°). Slight variations in estimated dip can result in relatively large thickness variations for the estimates of gaps in the succession.

## 3. Methods

### 3.1. Paleomagnetism

Samples were collected during fieldwork in 2015. Samples for magnetostratigraphy were taken on average every 50 cm. Conventional paleomagnetic cores (25 mm Ø) were collected using a gasoline-powered motor drill, and oriented using a magnetic compass. Directions were corrected for a present-day declination (International Geomagnetic Reference Field) of 7°. Cores were cut into specimens of ~22 mm long. A total of 254 specimens were subjected to stepwise thermal demagnetisation, and 304 were demagnetised using alternating field (AF) demagnetisation. Thermal demagnetisation was performed by progressive heating in a shielded furnace for 1 h, taking steps of 20–80 °C, up to 300 °C. After reviewing this procedure, more samples were demagnetised using steps of 20 °C up to 240 °C. AF demagnetisation was performed using a custom-built automated system, with steps of 2–20 mT, up to 100 mT (Mullender et al., 2016). Subsequently, the demagnetisation strategy was aimed at taking more steps below 40 mT, as magnetic signals were very weak. After each demagnetisation step, the natural remanent magnetisation (NRM) was measured on a 2G Enterprise horizontal cryogenic magnetometer equipped with three DC SQUIDS (noise level $3\times 10^{-12}$ $Am^2$). The 'per component' protocol (Finn and Coe, 2016; Mullender et al., 2016; Stephenson, 1993) was used, in which AF demagnetisation is applied per axis, after which the sample is measured. This protocol is used to prevent gyroremanent magnetisation, which can occur if greigite is present.

Vectors were calculated using principal component analysis (Kirschvink, 1980) on Zijderveld diagrams (Zijderveld, 1967) in the interpretation portal of Paleomagnetism.org (Koymans et al., 2016). Declinations and inclinations were calculated for pre-tilt (TC) and post-tilt (NOTC) signals. Mean directions were calculated using Fisher statistics (Fisher, 1953). We determined great circles for two components with overlapping blocking temperatures or coercivity. Lines and planes were determined following an eigenvector approach (Kirschvink, 1980). We use the method of McFadden and McElhinny (1988) to determine great circle solutions.

### 3.2. Rock-magnetic measurements

Thermomagnetic measurements of the induced magnetisation (J-T curves) in air, at high temperatures were conducted with a modified horizontal translation-type Curie balance with a sensitivity of $\sim 5\times 10^{-9} Am^2$ (Mullender et al., 1993). A field, cycling between 100 mT and 300 mT, was applied on powdered sediments (~70 mg). Multiple heating (6°/minute) and cooling runs (10°/minute) were performed.

### 3.3. Ar–Ar dating

The ash layer (sample code MKA) in the Maikop Group was sampled for $^{40}Ar/^{39}Ar$ dating and processed using standard mineral separation techniques. It was washed and dried, subsequently sieved through 90,

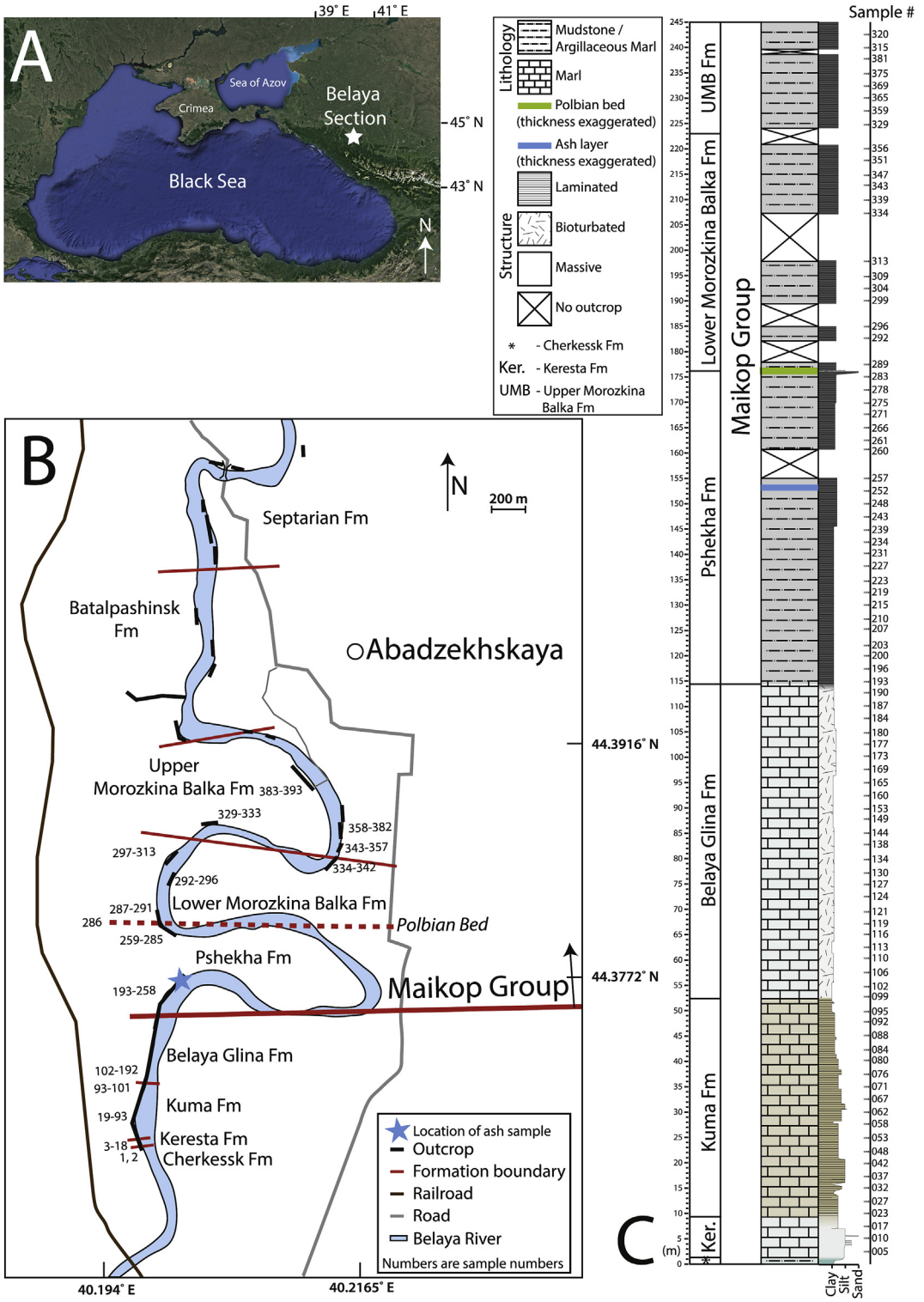


**Fig. 2.** A. Map of the location of the Belaya section (white star). B. Map of the Belaya River with outcrop locations, sample numbers and boundaries between different formations. C. Lithostratigraphic log with sample numbers, position of the ash layer and the Polbian bed (a distinctive white nannoplankton-marl bed in the black Maikop succession).

250 and 500 µm sieves and separated using heavy liquids (2.54, 2.59, 2.55, 2.60, 2.99 and 3.05 g/cm$^3$) to separate biotite minerals (no sanidine was found). Minerals were finally handpicked under a microscope and wrapped with standards in aluminium foil. Samples were irradiated during respectively 12 and 18 h in two irradiations (VU101 and VU107) at the Oregon State University Triga CLICIT facility, together with Fish Canyon Tuff sanidine as standard (FCs; 28.201 ± 0.023 Ma; Kuiper et al., 2008). After irradiation samples were loaded in Cu-trays and analysed using a 10-collector Helix-MC mass spectrometer with a customised extraction with SEAS NP10, St172 and Ti sponge getters and a Lauda cooler run at −70 °C. The used cup-configuration was either $^{40}$Ar on the H2 Faraday cup and $^{39}$Ar -$^{36}$Ar isotopes on compact discrete dynodes, or both $^{40}$Ar and $^{39}$Ar on respectively H2 and H1 Faraday. Gain calibration was done by

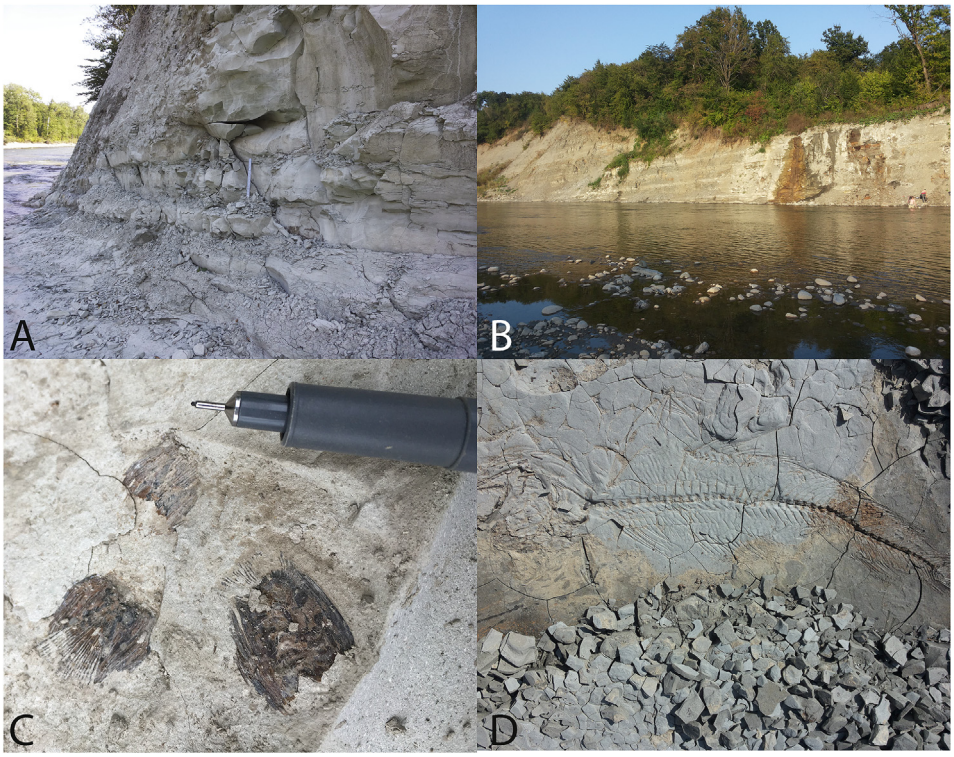


**Fig. 3.** A. Cycles in the Kuma Formation, ruler is 30 cm. B. Cycles in the Maikop Group, cliff is ~10 m high. C. Fish remains in the Kuma Formation. D. Fish fossil in the Maikop Group, fossil is ~30 cm long.

peakjumping $CO_2$ in dynamic mode on the different cups. Ages are calculated relative to the age of FCs reported in Kuiper et al. (2008) with decay constants of Min et al. (2000).

### 3.4. X-ray fluorescence

The compositions of 236 samples were measured, from the Cherkessk Formation up until the bottom part of the Lower Morozkina Balka Formation. Sample faces were smoothed with a ceramic knife to make flat surfaces. X-Ray fluorescence (XRF) measurements were conducted on a Thermo Scientific Niton XL3t SDD (900 GOLDD) Series XRF Analyser equipped with a 50 kV miniature X-ray tube with Ag anode and a Large Area Silicon Drift Detector under laboratory conditions with a steady flow of helium (~40 mm from the ball flow meter). Measuring time was 90 s in MINING mode. We refer to McIntosh et al. (2016) for an evaluation of this specific type of handheld XRF device, and Rowe et al. (2012) for an evaluation of handheld XRF measurements on geological materials.

### 3.5. Stable isotopes

Stable oxygen and carbon isotope ratios of bulk carbonate were measured for the top of the Keresta Formation, through the Kuma Formation to the bottom of the Belaya Glina Formation, on ~250–350 μg of freeze-dried and powdered sediment. Analyses were performed at Utrecht University using a Thermo Finnigan GasBench-II carbonate preparation device coupled to a Thermo Finnigan Delta-V isotope ratio mass spectrometer. Values for $\delta^{13}C$ and $\delta^{18}O$ are reported relative to the Vienna Pee Dee Belemnite (VPDB) standard. Analytical precision is ± 0.07‰ for $\delta^{13}C$ and ± 0.1‰ for $\delta^{18}O$, supported by NBS-19 and in-house standards.

### 3.6. Nannoplankton biostratigraphy

Nannoplankton samples were taken every third paleomagnetic sample. After a first zonation was established, the sample set was extended to locate the boundaries between different nannoplankton zones more precisely. Smear slides were made following the standard techniques described by Perch-Nielsen (1985) and Bown and Young (1998). Slides were observed under an OLYMPUS BH2 light microscope with cross polarised light and phase contrast illumination, at 900x and 1800x magnification. The standard scheme of Martini (1971) was adopted for this study.

## 4. Results

### 4.1. Paleomagnetism

#### 4.1.1. Thermomagnetic results

Powdered bulk material from different formations was measured in a horizontal translation type Curie balance (Mullender et al., 1993). The results show very small amounts of magnetic material in the Keresta interval (sample BE10 in Fig. 4), where negative values of magnetisation are measured, an expression of the diamagnetic properties of the glass holder. Magnetisation levels are weak throughout the section. All Curie balance diagrams show a decrease in magnetisation upon heating, with reversible behaviour up to ~400 °C. Each of the samples shows a significant increase in total magnetisation from around 400 °C to around 450 °C, after which the total magnetisation decreases again, and is nearly fully removed around 580 °C. A very slight change in slope around 680 °C can be observed for all samples, indicating the presence of minor amounts of hematite.

Pyrite, present in all samples (Fig. 4), is indicated by the increase in the magnetisation around 400 °C, the thermal zone of oxidation of pyrite to secondary magnetite (Passier et al., 1998).

#### 4.1.2. NRM intensity

NRM intensity at the first step is generally between 10 and 1000 μA/m throughout the section (see Fig. 7). In the Cherkessk Formation, magnetic susceptibility is around 150 μA/m, above which it drops up

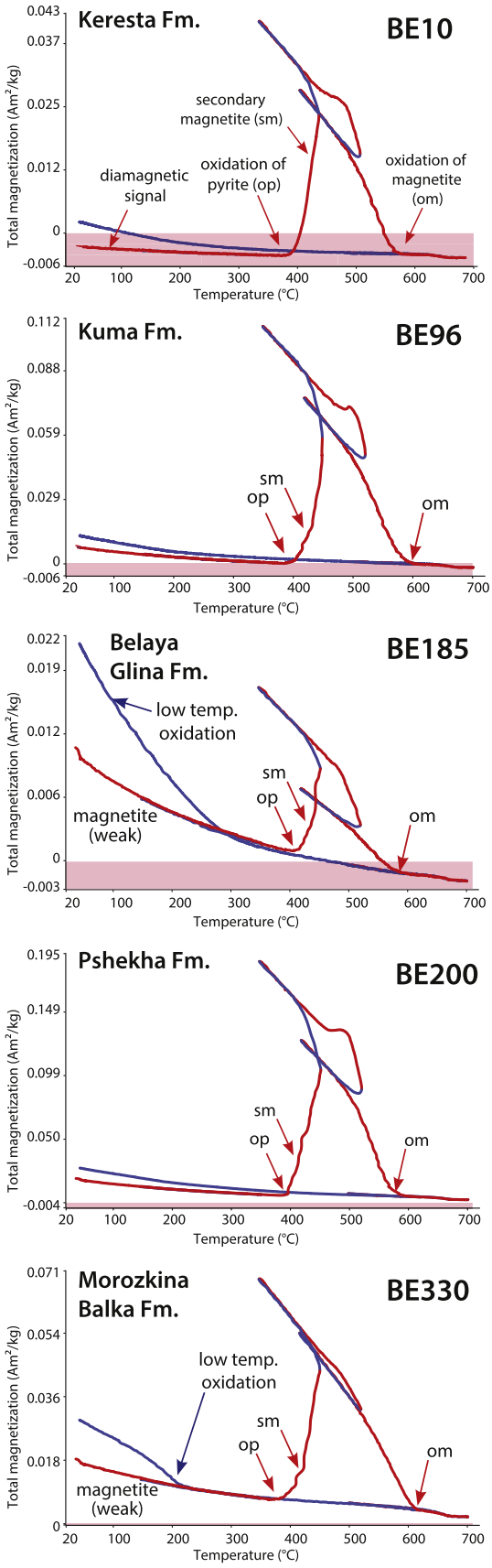


**Fig. 4.** Thermomagnetic runs using a Curie balance of samples of the different formations. Red lines indicate heating, blue lines indicate cooling. (For interpretation of the references to colour in this figure legend, the reader is referred to the Web version of this article.)

until the bottom of the Kuma Formation, where it reaches the lowest values of around 10 μA/m (around ~14 m). The interval from a stratigraphic height of 22 up to 26 m starts with a sharp increase in intensity and ends with a sharp decrease, and stands out with intensities of around 300 μA/m. Above the sharp fall, intensities gradually rise up until the top of the Kuma Formation, after which they decrease in the bottom of the Belaya Glina Formation. The Belaya Glina Formation shows intensity values of around 100 μA/m. Values begin to increase in the top of the Belaya Glina Formation. Intensities in the Maikop Group are slightly higher, and more variable than in the underlying formations.

#### 4.1.3. Characteristic remanent magnetisations

Demagnetisation patterns are generally not straightforward. Examples of representative Zijderveld diagrams are given in Fig. 5. Magnetic signals are generally weak (mostly tens to hundreds of μA/m), and most samples reach noise level after demagnetisation up to temperatures of 240 °C or fields of 40 mT. Fig. 5A–D shows characteristic remanent magnetisation (ChRM) components that were considered reliable (i.e. relatively straightforward demagnetisation towards the origin). Fig. 5A and D show normal polarities, 5B and 5C reversed polarities. Fig. 5B and C show that thermally demagnetised samples often display similar behaviour to AF-demagnetised samples. Fig. 5E shows a weak sample, exhibiting 'spaghetti plot' behaviour of which no ChRM could be determined. Fig. 5F and G show components that demagnetise relatively straightforwardly, but result in questionable directions that make them challenging for straightforward polarity interpretation. Fig. 5H and I are examples of samples with very shallow inclinations from the Maikop Group. Fig. 5J shows a Zijderveld diagram of a sample that does not demagnetise towards the origin, and has been interpreted using great circle analysis as shown in Fig. 5K.

Despite the low intensity of the samples, in some cases only just above noise level ($3 \times 10^{-12}$ A/m), normal and reverse polarities could be isolated in many cases. Samples show little to no low-temperature/low-coercivity overprint, but rather a more pervasive overprint which cannot always be removed. Samples commonly demagnetise towards the origin of Zijderveld diagrams. Samples that do not demagnetise towards the origin of Zijderveld diagrams were interpreted using great circle analysis. Several samples show a very low-temperature (up to 80 °C) component, while some reverse samples show overprints of up to 14 mT, but these are rare. Directions are usually interpreted using demagnetisation steps between 80 and 240 °C or 12–35 mT. Samples of the Keresta, Kuma and Belaya Glina Formations are noisier and have lower intensities compared to samples from the Maikop Group. All demagnetisation diagrams with interpreted directions are supplied in Directions.dir in the appendix. This file can be viewed in the interpretation portal of Paleomagnetism.org. All interpreted directions are plotted in an equal area projection in Fig. 6A.

Samples show elongated VGP distributions (Fig. 6B), which is typical for flattened sediments Tauxe and Kent, 2004. We use the E-I method (Tauxe et al., 2008) to detect and correct for inclination shallowing on directions of the Maikop Group (after tectonic correction). Fig. 6C shows the results of the unflattening procedure, which changes the average inclination from 41.89° before unflattening, to 52.09° after unflattening. The corrected inclination of 52.09° is still somewhat below the ~60° expected for the paleolatitude of the Belaya section around 35 Ma (Torsvik et al., 2012).

The interpreted polarity pattern is shown in Fig. 7. The base of the section shows normal polarities. Higher up into the Keresta Formation, the maximum angle of deviation (MAD) values increase, but samples still consistently give normal polarity directions. The base of the Kuma Formation gives mostly reverse polarities, which are partly derived from great circle analysis. MAD values for these directions are commonly > 10°. We tentatively assign a reverse polarity to the interval from 14 to 22 m. Above this level, up to around 45 m of stratigraphic height, no polarities could be assigned, due to the directions rapidly

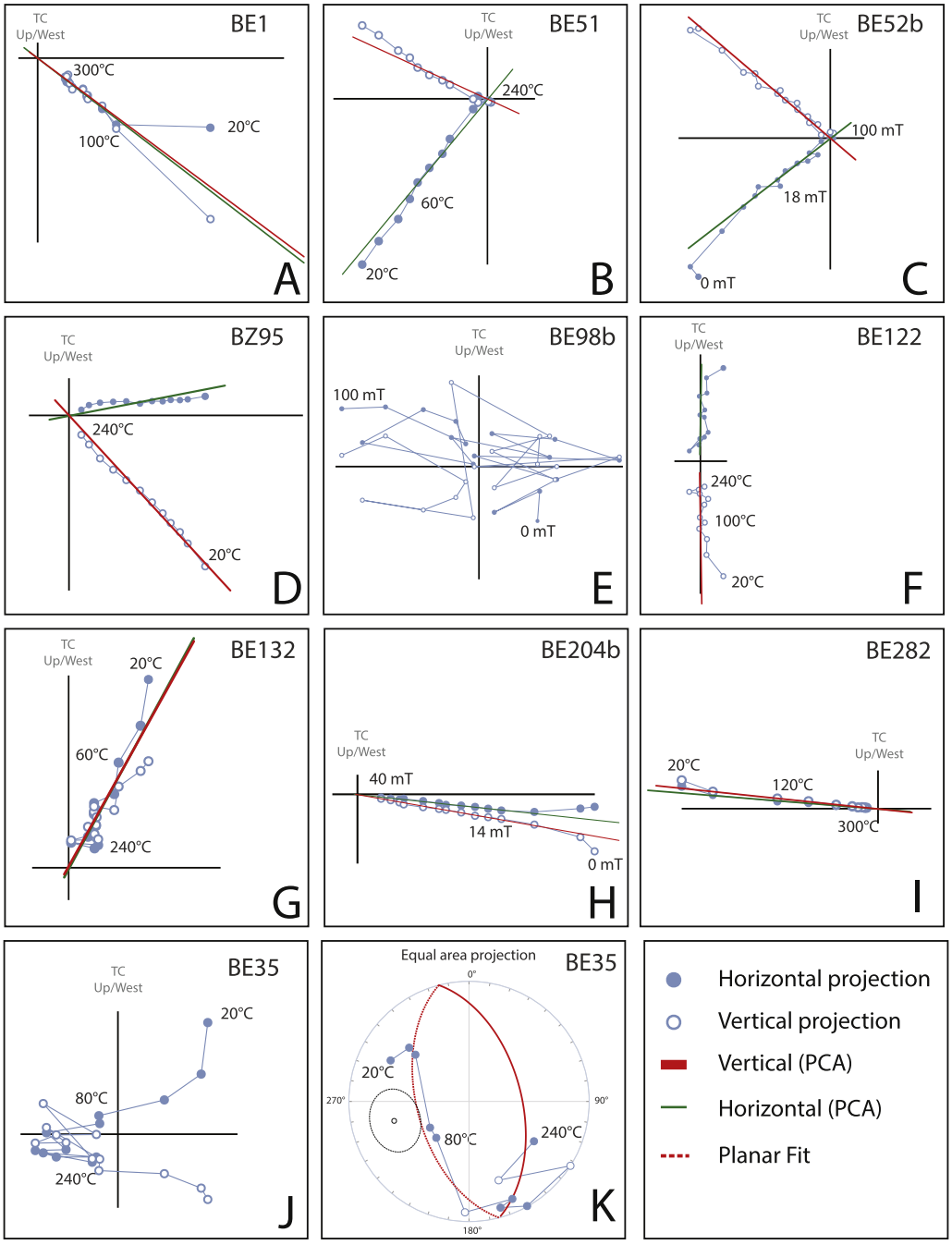


**Fig. 5.** Examples of representative Zijderveld diagrams, TC stands for tectonically corrected.

switching between normal and reversed, commonly with large uncertainties. From 45 up to 60 m, some great circle solutions give reverse polarities. However, directions predominantly show normal polarities in this interval, and we tentatively assign a normal polarity to this part of the section. In the Belaya Glina Formation, directions are generally associated with relatively large uncertainties, and polarities are mixed. In the top of the Belaya Glina Formation, from a stratigraphic height of 106 m, directions show predominantly normal polarities up into the Pshekha Formation at around 132 m. This interval is characterised by relatively small MAD values (< 10°), and we assign a normal polarity to this interval. From 132 m up until 178 m, samples show predominantly reverse polarities associated with MAD values of < 5°. We assign a reverse polarity to this part of the section. From 182 to 185 m, samples show normal polarities, and we assign a normal polarity to this part. For the interval between 189 and 198 m, no polarity could be established due to the mixture of both normal and reverse directions. Between 202 and 214 m, samples show mostly reverse polarities associated with small MAD values, and we assign a reverse polarity. The part between 214 and 247 m shows consistently normal polarities, with the exception of two reverse polarity samples at 220 and 223 m.

No reliable polarity zonation could be established for most of the Keresta, Kuma and Belaya Glina formations (Fig. 7). Directions in the Maikop Group are generally better, as they show less conflicting polarities and have smaller MAD values.

### 4.2. Ar–Ar dating

Ar–Ar dating of the biotite grains was performed during one fusion experiment, in which several grains were fused together. Intensities are low, only 2–3 times above blanks. Radiogenic $^{40}Ar^{*}$ contents are high,

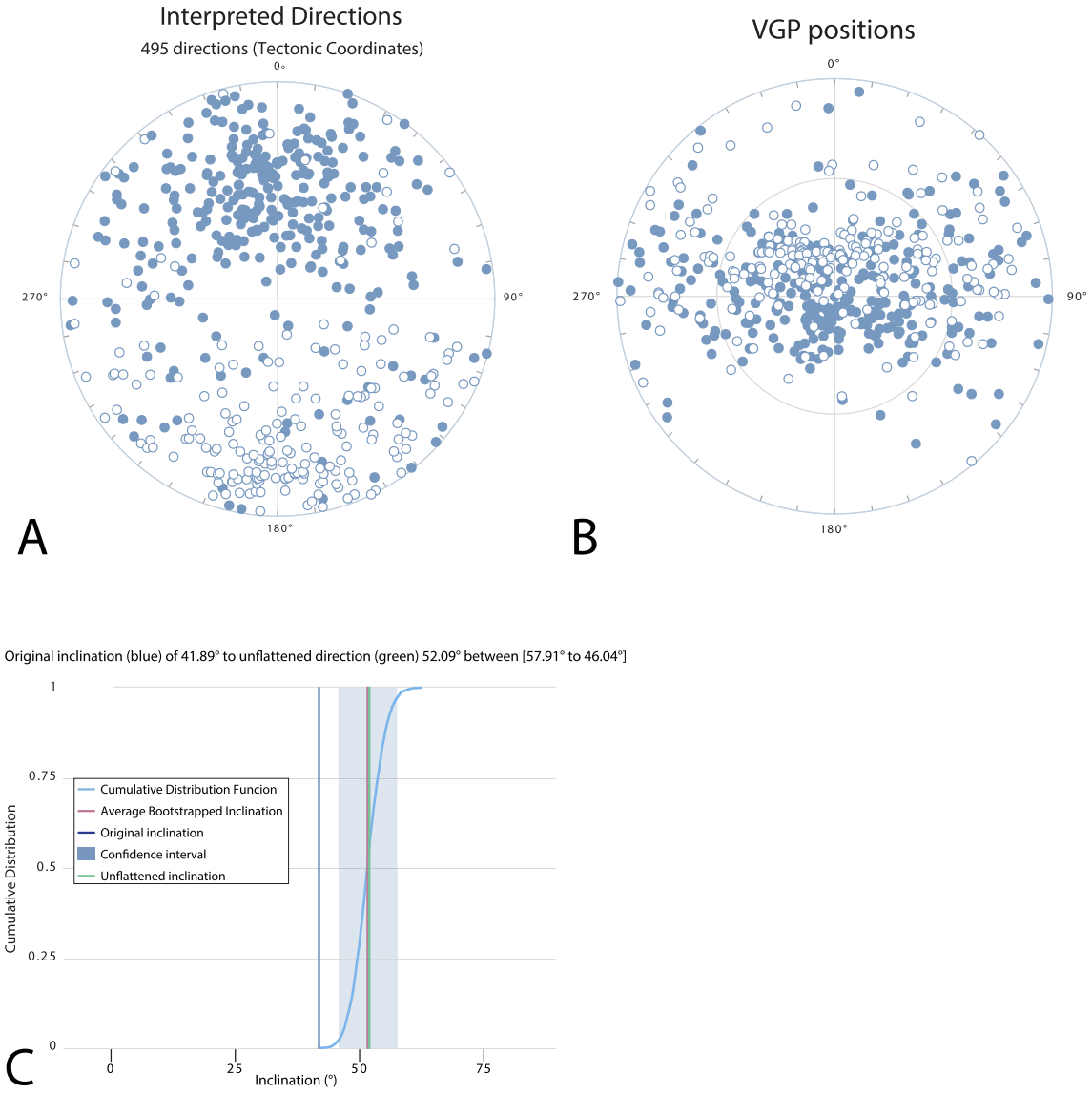


**Fig. 6.** Equal area projections of interpreted directions and VGP distributions. A. Interpreted directions of all samples. B. VGP positions of all interpreted samples. C. Results of unflattening inclinations for all interpreted directions and great circle solutions (after tectonic correction) with use of the E-I method (Tauxe et al., 2008).

above 93%, and isochrons show no deviations from atmospheric argon. Ar–Ar results are shown in Fig. 8. The biotite from the ash layer gives a plateau age of 33.2 ± 0.34 Ma (2σ). Results of the different fusion steps are plotted with 1σ errors in a density plot (Vermeesch, 2012), which shows a peak around an age of 33.12 Ma.

### 4.3. X-ray fluorescence

Elemental abundances mirror changes in lithology. Commonly, elemental abundances are normalised to aluminium or calcium (e.g. Tribovillard et al., 2006 and references therein). However, in this study this approach would result in large differences between the predominantly calcareous succession up to the Belaya Glina Formation (rich in calcium), and the clay-rich Maikop Group strata (rich in aluminium). Results are therefore not normalised, as shown in Fig. 9 (raw data are supplied in Table S2).

Generally, aluminium (Al) and calcium (Ca) mirror each other. Calcium abundances are low in the Cherkessk Formation, after which they increase to the highest values in the Keresta Formation and the bottom of the Kuma Formation. They subsequently drop to the middle of the Kuma Formation. This drop is accompanied by prominent enrichments in Al, vanadium (V) and molybdenum (Mo). Another decrease in Ca is present at the top of the Kuma Formation, but this is not accompanied by prominent enrichments in Al, V and Mo. Calcium content is variable throughout the Belaya Glina Formation, without obvious trends, and drops off into the Maikop Group sediments, where it is very low and variable without obvious trends. Values of Al and Ca are variable without apparent trends from the middle of the Kuma Formation upward. Aluminium contents are generally much higher in the Maikop Group.

Sedimentary Mo and V contents are sensitive to bottom water oxygen conditions (e.g., Tribovillard et al., 2006). In average shales, the Mo content is 1.3 ppm, and V is 130 ppm (Tribovillard et al., 2006, and references therein). Vanadium contents are high and show good agreement with Mo contents where these are above the detection limit. Molybdenum contents throughout the section are low, and in large parts of the section below the detection limit.

### 4.4. Stable isotopes

Fig. 9 shows bulk carbonate stable carbon ($\delta^{13}C$) and oxygen ($\delta^{18}O$) isotope records obtained for the bottom part of the section up into the

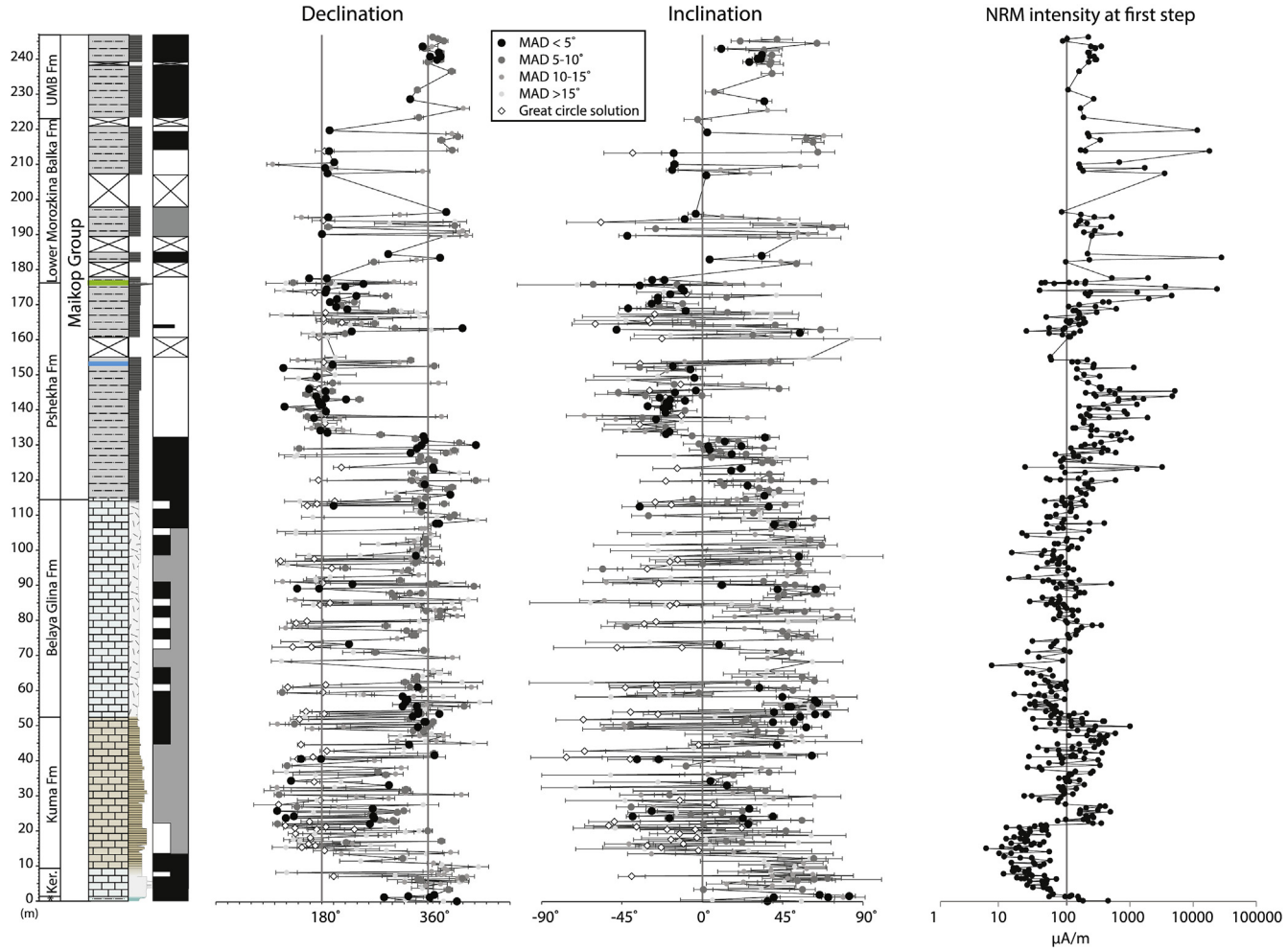


**Fig. 7.** Log of the section with the interpreted magnetostratigraphic polarity pattern, declination and inclination shown with MAD values as error bars and NRM intensity at the first step.

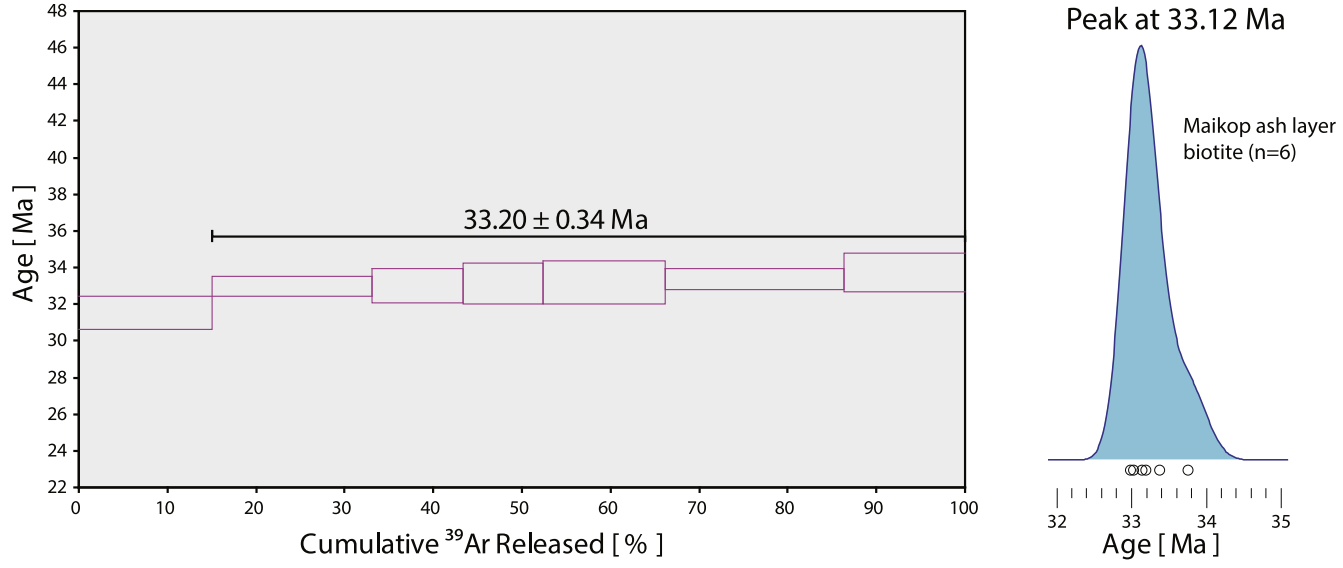


**Fig. 8.** Ar–Ar results of the ash layer in the Pshekhian Formation.

Pshekha Formation. Values for $\delta^{13}C$ show a large increase from the Cherkessk through the Keresta Formation into the Kuma Formation. Values vary around 1.5‰ for the upper part of the Kuma Formation and throughout the Belaya Glina Formation, with the exception of a negative excursion at the base of the Belaya Glina Formation. In the Pshekha Formation, carbon isotope values are generally lower and more variable.

Values for $\delta^{18}O$ in the section are generally very depleted and close

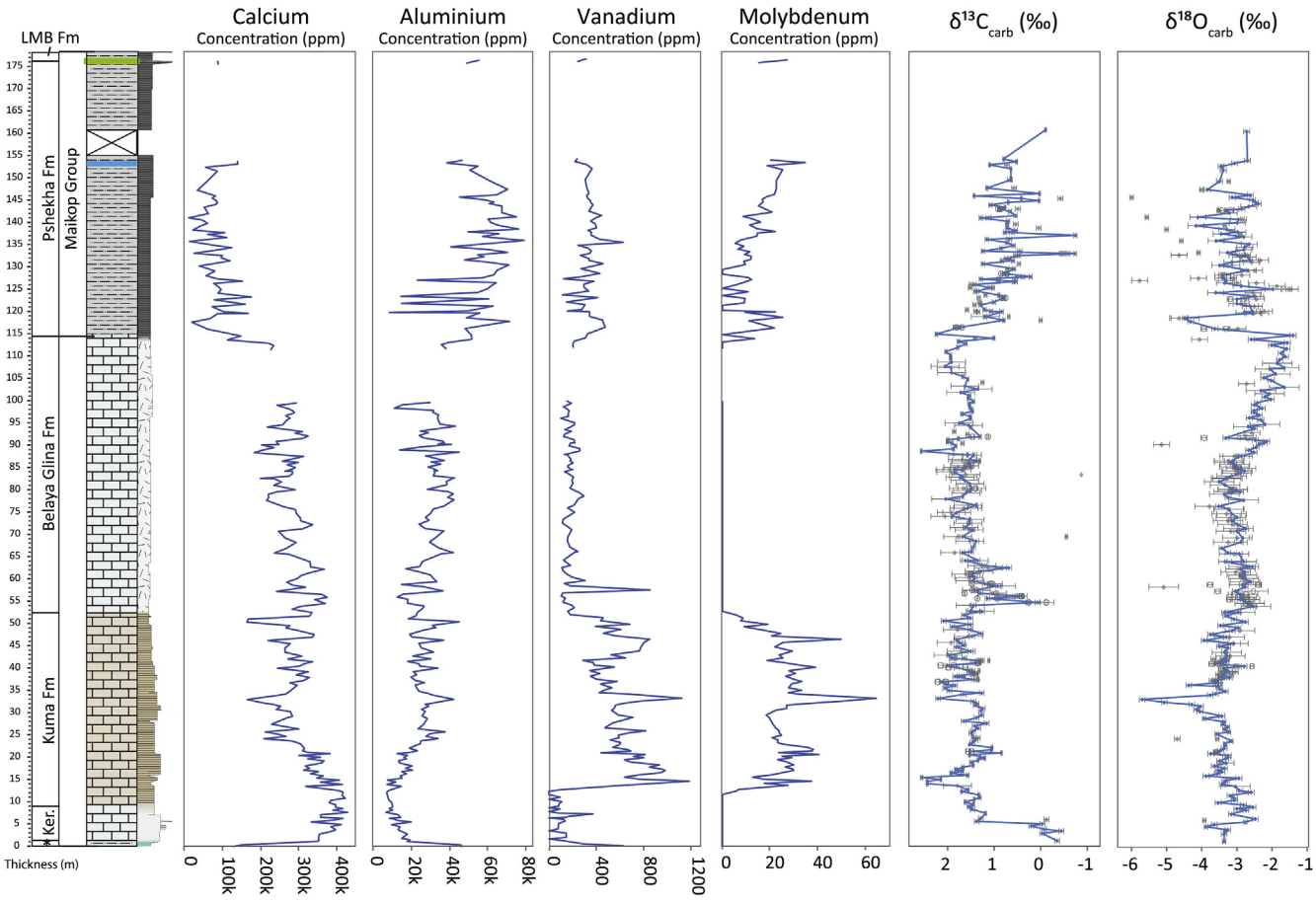


**Fig. 9.** Lithostratigraphic log of the section (* = Cherkessk Formation, Ker. = Keresta Formation, LMB = Lower Morozkina Balka Formation) with abundance of calcium, aluminium, vanadium and molybdenum in ppm based on handheld XRF measurements, and bulk carbonate carbon and oxygen isotope records (isotope measurements indicated with grey diamonds are less reliable results due to very low carbonate content. Some levels were measured multiple times, in which case the results were averaged. Original results for these levels are indicated by the grey circles.).

to the isotopic composition of meteoric waters (e.g. Gat, 1996), which might signify a groundwater-, or perhaps river water related diagenetic overprint. However, given the fairly stable background values in the studied interval we expect the diagenetic overprint to be relatively uniform so that the major trends and excursions are still preserved in the record. Values for $\delta^{18}O$ increase in the bottom part of the section, from the Cherkessk Formation through the Keresta Formation into the Kuma Formation, after which they gradually decrease. Throughout the lower half of the Kuma Formation, values are around −3.5‰. In the middle part of the Kuma Formation, a large negative oxygen isotope excursion is superimposed on the trend, reaching minimum values of −5.5‰ within a few metres. After this peak, values return to pre-excursion values within ~2 m, after which they gradually increase further to around −2.5‰ in the bottom of the Belaya Glina Formation. The lower half of the Belaya Glina Formation exhibits relatively stable values around −3‰, while in the upper half, values start to increase to around −1.5‰ around the Belaya Glina-Pshekha boundary. The boundary is marked by a sharp drop from around −1.5‰ to around −4.5‰, after which they return to −2.5‰ within a few metres. The rest of the Pshekha Formation is characterised by values around −3‰, but values are a lot more variable than in the other formations.

### 4.5. Nannoplankton biostratigraphy

Calcareous nannoplankton biostratigraphy is summarised in Table 1. Thick black lines designate marker species for nannoplankton zones (NP zones). For more detailed biostratigraphy, including molluscs, dinocysts and foraminifera, we refer to (Popov et al., 2019a).

In the Cherkessk Formation, the presence of zonal species of *Nannotetrina fulgens*, *Discoaster martinii* and a significant amount of *Nannotetrina cristata* indicate NP15 of *N. fulgens* (the upper part of zone CP13 according to Bukry, 1975, 1973).

In the Keresta Formation, mudstones and marlstones show a similar nannoplankton association, where a significant amount of *N. cristata* is present, but *N. fulgens* and *D. martinii* are absent from the Cherkessk-Keresta boundary upward. Such changes are typical for upper zone NP15 and lower zone NP16.

The lower part of the Kuma Formation contains a diverse association of nannoplankton, dominated by *Reticulofenestra* from the group "umbilica" *(R.hillae, R. callida, R. floridana, etc.)*. The presence of a significant amount of *Discoaster bifax*, *Discoaster distinctus, Discoaster binodosus, Discoaster deflandrei* and *Cyclococcolithus formosus*, along with occasional presence of *Chiasmolithus grandis* and *Discoaster tani nodifer*, indicates zone NP16 (or zone CP14, subzone CP14a). *Chiasmolithus solithus* (NP16) is observed constantly, but in small or medium amounts. Further up in the succession, large (14 μm) typical forms of *Reticulofenestra umbilica* appear, increasing in number upward. They become abundant in the upper part of zone NP17.

The upper part of the Kuma Formation contains large *R. umbilica* s.str., along with small reticulofenesters from the same group, and *Discoaster bisectum*. The background assemblage consists of D. *tani nodifer, D. binodosus, Discoaster saipanensis* and numerous *Coccolithus pelagicus, Cyclococcolithus formosus*, indicative of zone NP17 (CP14, subzone CP14b). The lower boundary of the zone is determined by the uppermost occurrence of *C. solitus* and the upper boundary by the lowermost occurrence of *Chiasmolithus oamaruensis*. In the upper part of

**Table 1**
Calcareous nannoplankton species. Thick black lines are marker species. Dotted lines indicate likely reworking, or non-continuous presence of species. Modified after Popov et al. (2019a).

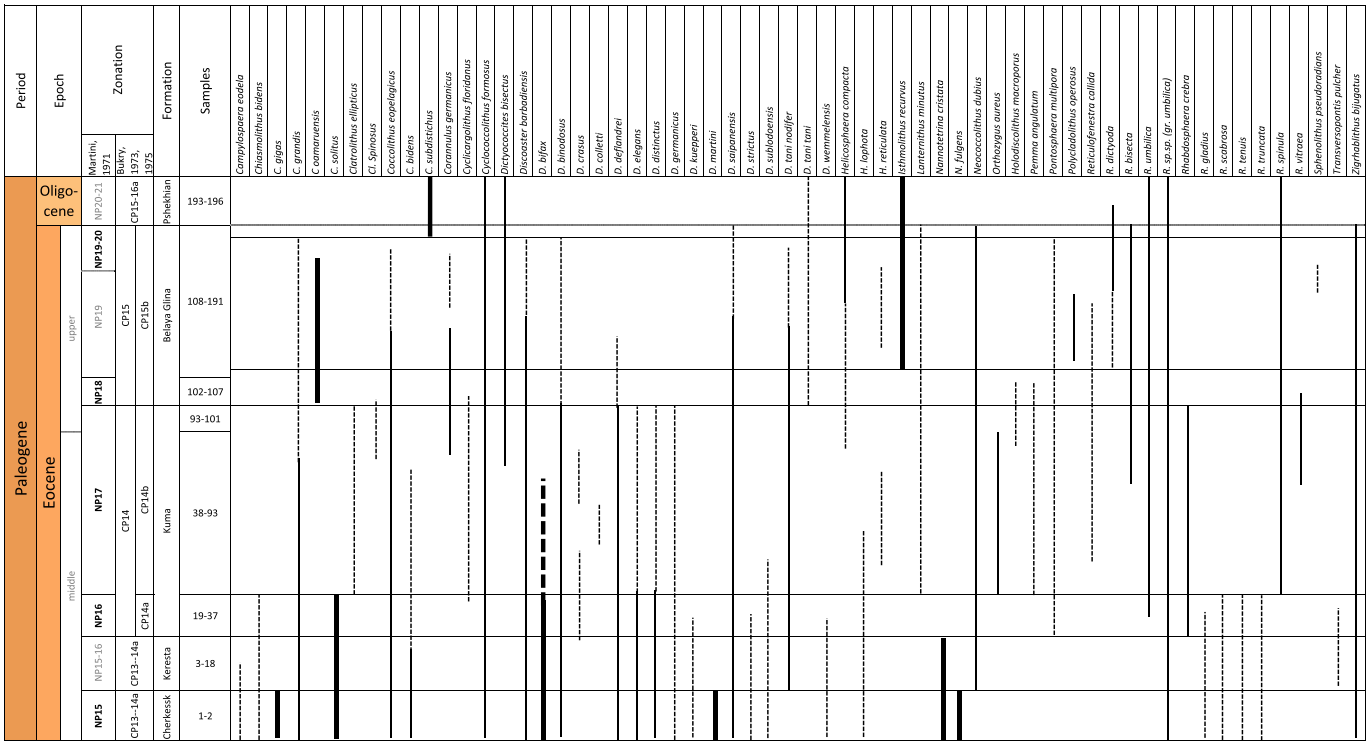


the Kuma Formation the number of nannoplankton fossils of the genus *Discoaster* decreases sharply.

In the basal part of the Belaya Glina Formation, large numbers of the zonal species *Chiasmolithus oamaruensis* appear together with *Dictyococcitus bisectus, Discoaster saipanensis, Corannulus germanicus, Discoaster tani tani* and *Helicosphaera reticulata*. This association corresponds to zone NP18. Zone NP19 is identified in the middle part of the Belaya Glina Formation, where *Isthmolithus recurvus* and *C. oamaruensis* are characteristic species. In some samples in the upper part of the Formation, *Sphenolithus pseudoradians* is present (zone NP20). The number of discoasters decreases towards the top of the Formation. A *Clausicoccus subdistichus* acme is observed in the uppermost part of the Belaya Glina Formation and the base of the Pshekha Formation, which is typical for the Eocene-Oligocene transition.

The dominant elements of the late Eocene association - *Coccolithus eopelagicus, D. bisectus* and *R. umbilica* – are continuously present in the lower parts of the Pshekha Formation, but their abundance is significantly reduced. The Eocene-Oligocene boundary (EOB) is located within zone NP21 (CP16a). Further up in the Pshekha Formation, the species *C. formosus* disappears and the nannoplankton association consists of numerous small reticulofenesters and *I. recurvus*. Large specimens of *R. umbilica* are observed only as single occurrences, indicating zone NP22.

A specific association of nannoplankton from marl of the Polbian bed consists of small *Reticulofenestra ornata*, numerous *Transversopontis fibula, Transversopontis* (also known as *Pontosphaera*) *pax* and *Transversopontis latus*. J. Krhovsky defined this association as belonging to zone NP23 (in Akhmetiev et al., 1995), while I. Tabachnikova interprets it as NP22-23 (Muzylev and Tabachnikova, 1987).

The non-calcareous laminated mudstones of the Lower Morozkina Balka Formation contain no nannoplankton. The base of the Upper Morozkina Balka Formation consists of an alternation of calcareous and non-calcareous mudstones, which belongs to zone NP24 on the basis of the top occurrence of *Transversopontis pygmaeus* and the base occurrence of *Helicosphaera recta* and *Cyclicargolithus abisectus*. Further upwards, abundant nannoplankton is present, including numerous small *Reticulofenestra* spp., *Cyclicargolithus floridanus, Dictyococcites bisectus, Pontosphaera multipora* and sporadically *Helicosphaera recta*.

## 5. Age constraints based on integrated stratigraphy

Fig. 10 shows a tentative correlation of the section to the geologic time scale (GTS2012, Gradstein et al., 2012), based on a combination of tie points. As we consider the nannoplankton biostratigraphy to be the most robust, we use this for first order age constraints.

The Cherkessk Formation comprises the lowermost 0.5 m of the section, and is of reported Ypresian-Lutetian age (Zakrevskaya et al., 2011). In the Kheu section (Kabardino-Balkaria), the Keresta Formation conformably overlies the Cherkessk Formation, while an unconformity separates the two formations further west (Radionova et al., 2003 and references therein). Calcareous nannoplankton assemblages indicate an age for the bottom part of the Belaya section around NP15-NP16 (~43 Ma in GTS2012). The combined presence of *Chiasmolithus solithus, Chiasmolithus gigas, Nannotetrina cristata, Nannotetrina fulgens* and *Discoaster bifax* suggests that there might be a slight reworking of nannoplankton representative of zone NP15 into zone NP16.

The Keresta Formation contains no additional nannoplankton species compared to the Cherkessk Formation, but lacks species *C. gigas, Discoaster distinctus* and *N. fulgens*. According to Radionova et al. (2003), the Keresta Formation of the Kheu section corresponds to nannoplankton zone NP15, which closely matches our results.

Calcareous nannoplankton assemblages are scarce in marker species in the Kuma Formation, although the bottom part contains *Chiasmolithus solitus* (NP9-NP16) and *Discoaster bifax* (NP16). Based on these species, and previous studies (e.g. Radionova et al., 2003), the lower part of the Kuma Formation is assigned to zone NP16 (43–40.5 Ma in GTS2012). Paleomagnetic results show that the lowermost 14 m of the section seems to have a normal polarity. We

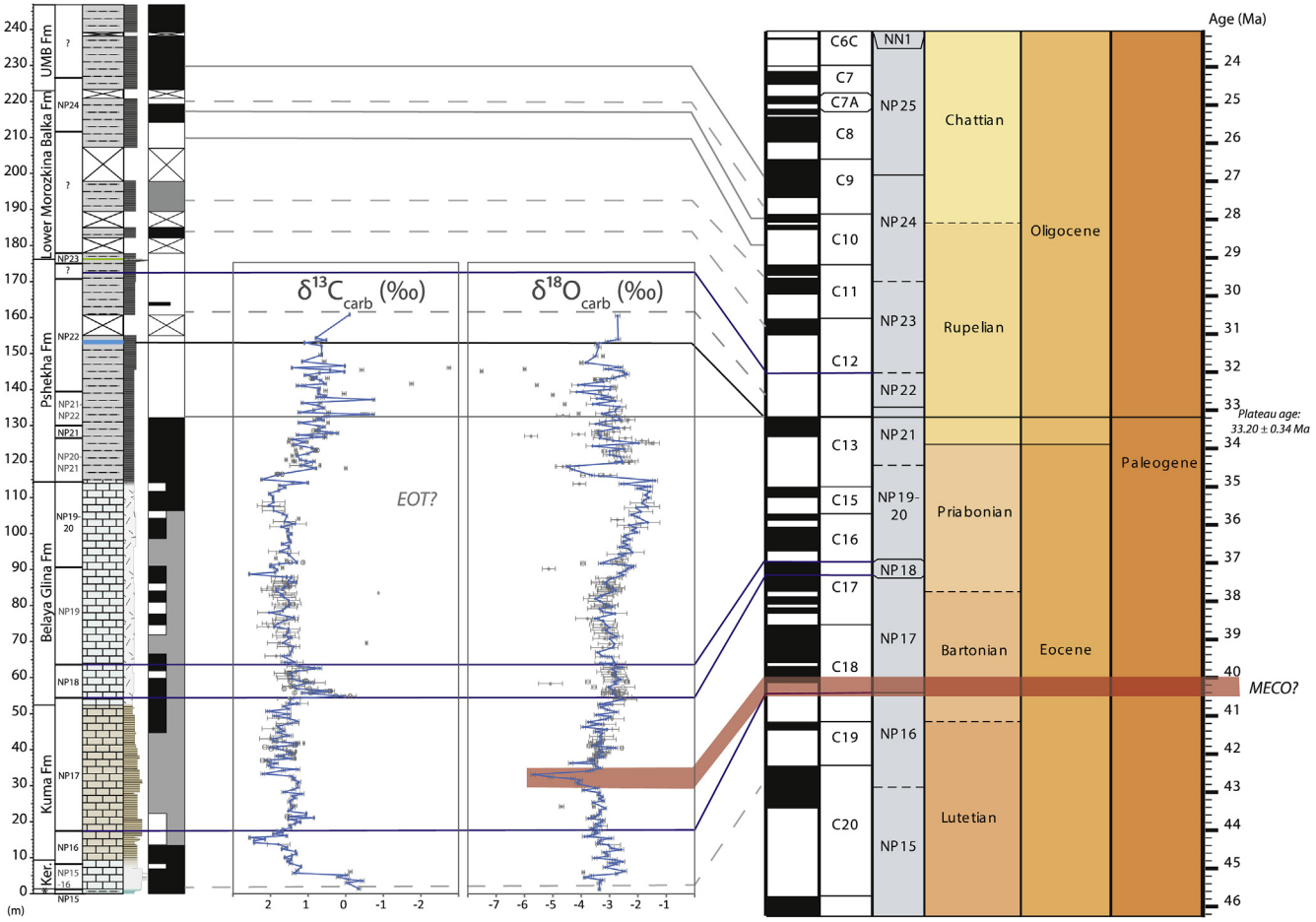


**Fig. 10.** Lithostratigraphic log of the section (* = Cherkessk Formation, Ker. = Keresta Formation, UMB = Upper Morozkina Balka Formation) with nannoplankton zonation and magnetostratigraphic interpretation (black represents normal polarity, grey unknown polarity and white reverse polarity). Also shown are the stable isotope records, with an indication where the Eocene-Oligocene Transition should roughly be in the section (EOT?). Blue lines indicate tie-points from the nannoplankton biostratigraphy that are used to correlate to the geologic timescale (TScreator). The red band indicates a negative oxygen isotope excursion that could be linked to the MECO (40.5–40.0 Ma). The black line correlates the radiometric age of the ash layer to the timescale. Grey lines indicate the hypothesised correlation of our magnetostratigraphy to magnetic chrons in the timescale. (For interpretation of the references to colour in this figure legend, the reader is referred to the Web version of this article.)

tentatively correlate this normal polarity zone to C20n. Above this part of the section, results are so mixed that we are unable to reliably determine the polarity up until the top of the Belaya Glina Formation. The top of the Kuma Formation is interpreted to be in NP17 (40.5–37.3 Ma in GTS2012), due to the presence of *Chiasmolithus oamaruensis* (NP18-NP22) in the lower part of the overlying Belaya Glina Formation. Although no marker species indicate zone NP17, part of the Kuma is likely in this zone, as sedimentation seems continuous and the bottom of the Belaya Glina formation is in zone NP18. The Kuma Formation thus corresponds for a large part to the Bartonian. The interval from ~28 to 35 m records a negative excursion in $\delta^{18}O$, which we tentatively correlate to the Middle Eocene Climatic Optimum (MECO; ~40 Ma; Bohaty et al., 2009; Sluijs et al., 2013), a period of widespread ocean warming superimposed on middle to late Eocene global cooling.

The bottom part of the Belaya Glina Formation corresponds to zone NP18 (37.3–37 Ma in GTS2012) due to the presence of *C. oamaruensis*, while the top corresponds to NP19-20 (37–34.5 Ma in GTS 2012) because of reported *I. recurvus*.

Our biostratigraphic data suggest that the Belaya Glina-Pshekha boundary is located within zone NP21, close to the Eocene-Oligocene boundary (33.9 Ma). We find the acme of *Clausicoccus subdistichus* in the top of the Belaya Glina Formation, which is the marker of zone NP21. This is in contrast with J. Krhovsky (in Akhmetiev et al., 1995), who mentions that the Belaya Glina-Pshekha transition occurs in NP19-20. We also encountered single specimens of characteristic species for the NP19-20 zone (*Discoaster barbadiensis* and *D. saipanensis*) in the *C. subdistichus* acme interval of the Pshekha Formation, which we interpret as reworked.

Paleomagnetic samples of the Maikop Group have a magnetic signal that is stronger than the lower part of the section, possibly due to increased detrital input, which is also reflected by higher Al contents. The magnetostratigraphic correlation of the Maikop Group to the GPTS is complicated however, due to gaps in the succession and the absence of nannoplankton marker species in parts of the sequence. The magnetostratigraphic pattern shows that the basal part of the Maikop Group is in a normal polarity zone, with nannoplankton species (126–130 m stratigraphic height) that are characteristic for zone NP21. We thus interpret the normal polarity zone to correspond to C13n. The bottom of this chron is unconstrained, as there should be a long reverse polarity interval (C13r) underneath it, but the paleomagnetic results do not show this. This implies that the Belaya Glina-Maikop transition likely has an age of around 33.7 Ma (the base of C13n), very close to the EOT.

## 6. Discussion

### 6.1. Age constraints

An additional age constraint is based on the Ar–Ar dating of the ash

layer in the Pshekha Formation, which gives a plateau age of 33.20 ± 0.34 Ma, and a density plot age of 33.12 Ma. An age of 33.20 Ma should correspond to the normal polarity chron C13n, according to the combined age model as adopted in GTS2012 (Gradstein et al., 2012). The age of 33.12 Ma would be only just above the base of chron C12r, at 33.16 Ma. However, according to our magnetostratigraphy, the ash layer is in a reverse polarity interval, and is located about 20 m above the transition from normal to reversed. We interpret this reverse polarity interval to correspond to C12r.

The GTS2012 gives two age models for the Eocene-Oligocene boundary which are significantly different (Vandenberghe et al., 2012), one model is based on cyclostratigraphy (age top C13n at 33.16 Ma) and the other is based on radio-isotopic constraints (age top C13n at 33.6 Ma). Our Ar–Ar age of 33.20/33.12 Ma of the ash layer 20 m within the reversed polarity interval is in good agreement with the radio-isotopic age model of GTS2012.

Sahy et al. (2017), however, performed U–Pb dating on zircons, which yielded results that are in agreement with the astronomically tuned Oligocene timescale. The U–Pb ages are then used to recalibrate ages for magnetic reversals and the Eocene-Oligocene boundary, which resulted in an age of 33.09 Ma for the top of chron C13n. Sahy et al. (2017) also discussed the discrepancy with the Ar–Ar based radio-isotopic model, and claimed that the biotite $^{40}Ar/^{39}Ar$ ages that support the late Eocene-Oligocene geomagnetic polarity time scale (GTS2012, Gradstein et al., 2012) are up to 0.5 Myr too old. Anomalously old biotite ages can result from $^{39}Ar$ recoil due to neutron irradiation, and/or presence of initial $^{40}Ar$. For a more detailed discussion on the complexities of $^{40}Ar/^{39}Ar$ geochronology on biotite, we refer to Sahy et al. (2017). We hypothesise that the biotite $^{40}Ar/^{39}Ar$ age of the Belaya ash suffers from the same problem and gives an anomalously old age.

Independent of the radiometric age model, the onset of Maikop sedimentation takes place in C13n, but the lower boundary of C13n is unconstrained. This means that the Belaya Glina-Pshekha transition could coincide with the Oi-1 eustatic sea-level drop, estimated at 50–60 m (Houben et al., 2012) in the bottom of C13n, or postdate it slightly. Macrofossil evidence suggests the latter, as shallow water benthic molluscs (including *Propeamussium fallax)* and echinoid remains appear in the uppermost part of the Belaya Glina Formation, indicating a sudden shift to shallower water depth. The base of the Pshekha Formation in the Belaya River section is conformable, and geochemical proxies (e.g., carbonate and total organic carbon (TOC) contents, Pristane/Phytane ratios - Sachsenhofer et al., 2017) show a rapid transition from the Belaya Glina Formation to the Pshekha Formation. This indicates that the study area remained subaquatic during the sea-level drop. If the largest sea-level drop already occurred in the Belaya Glina Formation, Oi-1 predates the onset of low oxygen conditions, indicating a small time lag between global cooling and the establishment of these conditions. Phytoplankton data suggest a short freshening event during the transition (Sachsenhofer et al., 2017). A composition of fossil leaves, pollen and spores together with high amounts of land plant biomarkers within the lower part of Pshekha Formation are another consequence of the sea-level drop and indicate proximity to dry land (Sachsenhofer et al., 2017).

The oxygen isotope pattern that is characteristic for the Eocene-Oligocene transition –three distinct steps showing increasing $\delta^{18}O$ (e.g. Katz et al., 2008) – is not recognized in the Belaya section. Instead, after the gradual rise of $\delta^{18}O$ in the upper half of the Belaya Glina Formation, oxygen isotopes show a sharp depletion instead of a sharp enrichment around the boundary with the Pshekha Formation. This might be related in part to a lithological overprint on the isotopes, potentially similar to the observed peak in the Kuma Formation, but might also indicate a difference in response of the epicontinental Paratethys versus the open ocean record. Ozsvárt et al. (2016) also report 'unexpectedly negative $\delta^{18}O$ values' which they link to possible alteration, or increased precipitation in the Paratethys, although patterns in their study are reported to be similar to the global deep-sea isotope records around the EOT.

### 6.2. Sediment accumulation rates

Using the lower end of C13n at 33.705 Ma as age for the Belaya Glina-Maikop boundary, and interpreting the most depleted $\delta^{18}O$ values in the Kuma Formation as peak MECO warming around 40.0 Ma (Bohaty et al., 2009), we estimate average sediment accumulation rates for the Kuma and Belaya Glina Formations of 1.3 cm/kyr. Cycles in the Belaya Glina Formation are about 20–30 cm thick, which, with a sedimentation rate of around 1.3 cm/kyr, would match quite well with climatic precession cyclicity that has a periodicity of around 23 kyr.

Assuming constant sedimentation rates for the lower part of the section up to the Belaya Glina-Pshekha boundary of 1.2 cm/kyr, and using the oxygen isotope excursion at 40.0 Ma (~33 m) as a tentative tie point, we estimate ages for the boundaries between formations. The bottom of the section corresponds to an age of ~43 Ma (42.8 Ma). Further extrapolation of this sedimentation rate places the Cherkessk-Keresta boundary at an age of 42.7 Ma, the Keresta-Kuma boundary at 42.1 Ma, and the Kuma-Belaya Glina boundary at 38.4 Ma.

### 6.3. Oxygen-depleted episodes

The succession along the Belaya River shows two episodes that are linked to intensified oxygen depletion, the lower one in the Kuma Formation, and the upper one in the Maikop Group. If sediments show enrichment in V but no enrichment in Mo, oxygen-depleted conditions without free $H_2S$ in the water column are assumed. When sediments show enrichment in both elements, euxinic conditions (i.e., oxygen depletion accompanied by free $H_2S$ in the water column) are inferred (Tribovillard et al., 2006).

#### 6.3.1. Kuma Formation

The earliest oxygen-depleted episode occurs in the Kuma Formation, which shows high TOC contents, and enrichment in both V and Mo, indicating euxinic conditions. The TOC in the Kuma Formation of the Belaya River is up to 6% (Sachsenhofer et al., 2018), while in the Bakhchisaray section in Crimea, even higher values of 7.5% are reported (Beniamovski et al., 2003). Although we did not find any ash layers in the Kuma Formation along the Belaya River, many bentonites are reported from Kuma sections both to the west (Bakhchisaray section, Crimea; Beniamovski et al., 2003) and east (Kheu River section, Kabardino-Balkaria; Beniamovski et al., 2003). Also in the Kura basin of Azerbaijan, extensive ash deposits of middle Eocene age are found (Lerche et al., 1997). Beniamovski et al. (2003) suggested that the oxygen depletion in the Kuma Formation is linked to a high input of nutrients caused by volcanism in the region. Numerous bentonite interlayers are known in the Ezet and Kurtysh Formations of Turkmenistan, and similarly aged sediments of Ustyurt (Kazakhstan) (Muzylöv, 1996). The thickness of these interlayers is up to several decimetres. Industrial deposits of bentonites (thickness of several meters) are described in the Oglanlyn suite in Turkmenistan (Muzylöv, 1996). Throughout the Lutetian and Bartonian, ash accumulations are linked to observed increases in TOC, suggesting that volcanism was linked to increased productivity and/or preservation of organic material in the basin (Muzylöv, 1996). The most likely candidate for this volcanism is the Neotethys continental arc in Iran, which experiences a flare-up stage around the middle Eocene (e.g. Verdel et al., 2011), although we cannot exclude increased runoff as another mechanism for increasing productivity in the Kuma basin.

The fundamental difference between the Kuma and Maikop basins is the normal oceanic salinity of the Peri-Tethys basin, which is deduced from planktonic foraminifera and nannoplankton data (Popov et al., 2019a). The fact that microfauna was mainly planktonic during Kuma deposition indicates unfavourable bottom-water conditions at times (e.g. Popov et al., 2019a), but the oxygen depletion was interspersed by

oxic episodes (e.g. Muzylöv, 1996; Shcherbinina and Gavrilov, 2007).

The presence of in situ molluscs (small oysters of *Liostrea simplex* Desh.; Popov et al., 2019a) in the middle and at the top of the Kuma Formation, together with benthic foraminifers and a noticeable bioturbation of the sediments is evidence of a periodic restoration of bottom-water ventilation, which was favourable for benthic fauna.

*6.3.2. Maikop Group: oxygen depletion and the EOT*

Similar to the Kuma Formation, euxinia in the Maikop Group strata is based on simultaneous enrichment in V and Mo and on biotic data, but TOC contents are much lower than in the Kuma Formation: up to 2.5% for the Pshekha Formation and up to 3.5% for the Lower Morozkina Balka subformation (Sachsenhofer et al., 2017). In addition, the visual appearance of these sediments is markedly different from those of the Kuma Formation.

Oxygen depletion in the Maikop Group lasted for almost 20 million years, from the Early Oligocene until the Middle Miocene (~14.9 Ma; Palcu et al., 2019), with a few short episodes in which oxygen was available in the water column (Sachsenhofer et al., 2017). In contrast with the Kuma Formation, the oxygen depletion in the Maikop Group is generally not associated with increased volcanism, and the amount of reported ashes from literature in the Rupelian is significantly smaller compared to the Lutetian and Bartonian (e.g. Muzylöv, 1996). Oxygen depletion in the Maikop Group is commonly interpreted as a result of changes in basin configuration. More specifically the change from the Peri-Tethys, which had connections to the open ocean, to the Paratethys, which developed an endemic fauna in response to limited communication. The Maikop basin was not fully marine and salinity was unstable (e.g. Popov and Studencka, 2015; Sachsenhofer et al., 2017). A dysoxic regime was likely the result of strong haline stratification in the Paratethys. The limits of the Paratethys can be traced by looking at the nature of Oligocene deposits along the borders of the basin. Sediments of the Maikop Group were deposited around the Black Sea and Caspian Sea, in the Lesser Caucasus the Central Kopet Dagh. The basin was bounded by the Pontides, Lesser Caucasus and the Alborz mountains. Connections of the Paratethys towards the south are often interpreted through the Lesser Caucasus (Rögl, 1999), but upper Paleogene connections were likely limited to the middle Priabonian, based on biogeographical data (Popov et al., 2001, 2004a).

The connection of the Paratethys to the Atlantic and Mediterranean through the North Alpine foreland basin (NAFB) was still open around the EOT. This connection closed around 33.15 Ma (van der Boon et al., 2018), corresponding to halfway up the Pshekha Formation in the Belaya section. Restriction of the Paratethys in response to sea-level changes around the EOT must thus have been related to limitation of a large gateway, after which only relatively small gateways remained open. This restriction then limited ventilation of the basin, leading to basin-wide low oxygen conditions, while the marine character of the Paratethys was kept intact. Only when remaining connections became closed or significantly reduced in size, did the marine character disappear, the basin become brackish and endemic fauna develop. The Paratethys showed the first endemic, brackish fauna during the Solenovian in nannoplankton zone NP23 (Popov and Studencka, 2015), which corresponds to the interval around the Polbian bed in the Belaya section. We assume that the closure or a significant decrease in the depth of the connection with the North Atlantic through Poland, Germany and Denmark may have led to almost complete isolation of the Paratethys during the Solenovian. During the Chattian this connection was restored, since the Late Oligocene fauna of Paratethys (as well as the Early Oligocene), closely resembles the benthic fauna of North Sea basins. Mediterranean species in the Paratethys began to appear only from the beginning of the Miocene (Popov et al., 2004b).

## 7. Conclusions

The sedimentary succession along the Belaya River in Adygea, Russia provides a continuous record of sediments from the middle Eocene up into mid-Rupelian (Solenovian), recording sedimentation through an interval with important climatic events. A middle Eocene age for the lower part of the succession is established mainly from calcareous nannoplankton biostratigraphy. Magnetostratigraphy for the lower part of the section up to the boundary of the Maikop Group could not be reconstructed, due to the low quality of magnetic signals. Magnetostratigraphy in the Maikop Group shows a normal polarity chron for the base of the Maikop, together with nannoplankton characteristic of zone NP21. We thus interpret this normal polarity zone to correspond to C13n. The base of the Maikop Group is close to the Eocene-Oligocene boundary. However, as the Eocene-Oligocene boundary occurs in a reversed interval, the base of the Maikop Group does not correspond exactly to the EOB. Furthermore, we do not find a long reverse polarity zone underneath the Maikop Group, due to the low quality of the magnetic signals, and the bottom of C13n is thus unconstrained. We hypothesise that the base of the Maikop Group slightly postdates the Oi-1 sea-level drop of approximately 50–60 m, based on the occurrence of shallow water benthic molluscs and echinoid remains that indicate a sudden shallowing in the top of the Belaya Glina Formation. Reconstructing the polarity pattern for the Polbian–Lower Morozkina Balka interval is complicated by gaps in the succession, low quality of magnetic signals and absence of nannoplankton data for parts of the succession. The succession along the Belaya River shows two oxygen-depleted episodes, the lower one in the Kuma Formation and the upper one in the Maikop Group. Low oxygen conditions in the Kuma Formation are possibly linked to volcanism in the Neotethys region, although no bentonites are found in the Belaya section. Oxygen depletion in the Maikop Group lasts for almost 20 million years, and is likely linked to a semi-closed basin configuration with sharp haline stratification.

## Declaration of competing interest

The authors declare that they have no conflict of interests.

## Acknowledgements

This work was financially supported by the Netherlands Organization for Scientific Research (NWO) [grant 865.10.011] of WK and the Russian Foundation for Basic Research (project no. 17-05-00047). We thank Michael Morton, Stephen Vincent, Sarah Davies, Larisa Golovina, Tatiana Pinchuk, Alexandra Rylova, Chris van Baak, Arjen Grothe, Suzhen Liu, Niels van Helmond and Kevin Vis for help in the field and valuable discussions. We thank Roel van Elsas for help with mineral separation for $^{40}Ar/^{39}Ar$ dating, and Camille Chapeland for measuring XRF. We thank three anonymous reviewers and editor Thomas Algeo for their detailed comments that have greatly improved the manuscript.

## Appendix A. Supplementary data

Supplementary data to this article can be found online at https://doi.org/10.1016/j.palaeo.2019.109395.

## References

Adams, D.D., Hurtgen, M.T., Sageman, B.B., 2010. Volcanic triggering of a biogeochemical cascade during oceanic anoxic event 2. Nat. Geosci. 3, 201–204.

Akhmetiev, M.A., Popov, S.V., Krhovsky, J., Goncharova, I.A., Zaporozhets, N.I., Sychevskaya, E.K., Radionova, E.P., 1995. Palaeontology and stratigraphy of the eocene–miocene sections of the western pre-caucasia. Excursion guideb. Moscow. Russ. Comm. Int. Geol. Correl. Program. Paleontol. Inst.

Akhmetiev, M.A., Zaporozhets, N.I., Benyamovskiy, V.N., Aleksandrova, G.N., Iakovleva, A.I., Oreshkina, T.V., 2012. The paleogene history of the western Siberian seaway - a connection of the Peri-Tethys to the Arctic Ocean. Aust. J. Earth Sci. 105, 50–67.

Bachmann, G.H., Müller, M., 1992. Sedimentary and structural evoluion of the German molasse basin. Eclogae Geol. Helv. 85, 519–530.

Beniamovski, V.N., Alekseev, A.S., Ovechkina, M.N., Oberhänsli, H., 2003. Middle to upper Eocene dysoxic-anoxic Kuma Formation (northeast peri-Tethys): biostratigraphy and paleoenvironments. Geol. Soc. Am. Spec. Pap. 369, 95–112.
Benyamovskiy, V.N., 2012. A high resolution Lutetian-Bartonian planktonic foraminiferal zonation in the Crimean-Caucasus region of the northeastern Peri-Tethys. Aust. J. Earth Sci. 105, 117–128.
Bohaty, S.M., Zachos, J.C., Florindo, F., Delaney, M.L., 2009. Coupled greenhouse warming and deep-sea acidification in the middle Eocene. Paleoceanography 24, 1–16.
Bown, P.R., Young, J.R., 1998. Techniques. In: Calcareous Nannofossil Biostratigraphy. Chapman and Hall, London, pp. 16–28.
Bukry, D., 1973. Low-latitude biostratigraphic zonation. Initial reports deep sea drill. Projet 15, 685–703.
Bukry, D., 1975. Coccolith and silicoflagellate stratigraphy, northwestern pacific ocean, deep sea drilling project leg 32. Initial reports deep sea drill. Projet 32, 677–701.
Dawber, C.F., Tripati, A.K., Gale, A.S., MacNiocaill, C., Hesselbo, S.P., 2011. Glacioeustasy during the middle Eocene? Insights from the stratigraphy of the hampshire basin, UK. Palaeogeogr. Palaeoclimatol. Palaeoecol. 300, 84–100.
Ershov, A.V., Brunet, M.-F., Korotaev, M.V., Nikishin, A.M., Bolotov, S.N., 1999. Late Cenozoic burial history and dynamics of the Northern Caucasus molasse basin: implications for foreland basin modelling. Tectonophysics 313, 219–241.
Ershov, A.V., Brunet, M.F., Nikishin, A.M., Bolotov, S.N., Nazarevich, B.P., Korotaev, M.V., 2003. Northern Caucasus basin: thermal history and synthesis of subsidence models. Sediment. Geol. 156, 95–118.
Finn, D.R., Coe, R.S., 2016. A new protocol for three-axis static alternating field demagnetization of rocks. Geochem. Geophys. Geosyst. 17, 1815–1822.
Fisher, R., 1953. Dispersion on a sphere. Proc. R. Soc. Lond. 217, 295–305.
Gat, J.R., 1996. Oxygen and hydrogen isotopes in the hydrologic cycle. Annu. Rev. Earth Planet Sci. 24, 225–262.
Giorgioni, M., Jovane, L., Rego, E.S., Rodelli, D., Frontalini, F., Coccioni, R., Catanzariti, R., Özcan, E., 2019. Carbon cycle instability and orbital forcing during the middle Eocene climatic optimum. Sci. Rep. 9, 1–10.
Gradstein, F.M., Ogg, J.G., Schmitz, M., 2012. The Geologic Time Scale 2012. Elsevier.
Grossheim, V.A., 1960. The paleogene of the northwestern Caucasus. Tr. Krasn. Fil. VNIGRI. Moscow Gostoptekhizdat 4.
Guliyev, I.S., Tagiyev, M.F., Feyzullayev, A.A., 2001. Geochemical characteristics of organic matter from Maikop rocks of eastern Azerbaijan. Lithol. Miner. Resour. 36, 280–285.
Houben, A.J.P., van Mourik, C.A., Montanari, A., Coccioni, R., Brinkhuis, H., 2012. The Eocene-Oligocene transition: changes in sea level, temperature or both? Palaeogeogr. Palaeoclimatol. Palaeoecol. 335–336, 75–83.
Hudson, S.M., Johnson, C.L., Efendiyeva, M.A., Rowe, H.D., Feyzullayev, A.A., Aliyev, C.S., 2008. Stratigraphy and geochemical characterization of the oligocene–miocene Maikop series: implications for the paleogeography of eastern Azerbaijan. Tectonophysics 451, 40–55.
Johnson, C.L., Hudson, S.M., Rowe, H.D., Efendiyeva, M.A., 2010. Geochemical constraints on the Palaeocene-Miocene evolution of eastern Azerbaijan, with implications for the South Caspian basin and eastern Paratethys. Basin Res. 22, 733–750.
Jovane, L., Coccioni, R., Marsili, A., Acton, G., 2009. The late Eocene greenhouse-icehouse transition: observations from the Massignano global stratotype section and point (GSSP). Geol. Soc. Am. Spec. Pap. 452, 149–168.
Katz, M.E., Miller, K.G., Wright, J.D., Wade, B.S., Browning, J.V., Cramer, B.S., Rosenthal, Y., 2008. Stepwise transition from the Eocene greenhouse to the Oligocene icehouse. Nat. Geosci. 1, 329–334.
Kirschvink, J.L., 1980. The least-squares line and plane and the analysis of palaeomagnetic data. Geophys. J. Int. 62, 699–718.
Koymans, M.R., Langereis, C.G., Pastor-Galán, D., van Hinsbergen, D.J.J., 2016. Paleomagnetism.org: an online multi-platform open source environment for paleomagnetic data analysis. Comput. Geosci. 93, 127–137.
Kuiper, K.F., Deino, A., Hilgen, F.J., Krijgsman, W., Renne, P.R., Wijbrans, J.R., 2008. Synchronizing rock clocks of Earth history. Science 320, 500–504.
Laskarev, V., 1924. Sur les équivalents du sarmatien supérieur en Serbie, in: Receuil de Traveaux Offert à M. Jovan Cvijic Par Ses Amis et Collaborateurs a l'occasion de Ses Trente-Cinq Ans de Travail Scientifique.
Lerche, I., Ali-Zadeh, A., Guliyev, I., Bagirov, E., Nadirov, R., Tagiyev, M., Feizullayev, A., 1997. South Caspian Basin: Stratigraphy, Geochemistry and Risk Analysis.
Martini, E., 1971. Standard Tertiary and Quaternary calcareous nannoplankton zonation. In: Proceedings of the Second Planktonic Conference.
McFadden, P.L., McElhinny, M.W., 1988. The combined analysis of remagnetization circles and direct observations in palaeomagnetism. Earth Planet. Sci. Lett. 87, 161–172.
McIntosh, K.G., Guimarães, D., Cusack, M.J., Vershinin, A., Chen, Z.W., Yang, K., Parsons, P.J., 2016. Evaluation of portable XRF instrumentation for assessing potential environmental exposure to toxic elements. Int. J. Environ. Anal. Chem. 96, 15–37.
McQuarrie, N., van Hinsbergen, D.J.J., 2013. Retrodeforming the Arabia-Eurasia collision zone: age of collision versus magnitude of continental subduction. Geology 41, 315–318.
Miller, K.G., Wright, J.D., Katz, M.E., Wade, B.S., Browning, J.V., Cramer, B.S., Rosenthal, Y., 2009. Climate threshold at the Eocene-Oligocene transition: antarctic ice sheet influence on ocean circulation. Geol. Soc. Am. Spec. Pap. 452, 169–178.
Min, K., Mundil, R., Renne, P.R., Ludwig, K.R., 2000. A test for systematic errors in 40 Ar/39 Ar geochronology through comparison with U/Pb analysis of a 1.1-Ga rhyolite. Geochem. Cosmochim. Acta 64, 73–98.
Mullender, T.A.T., Frederichs, T., Hilgenfeldt, C., de Groot, L.V., Fabian, K., Dekkers, M.J., 2016. Automated paleomagnetic and rockmagnetic data acquisition with an inline horizontal "'2G"' system. Geochem. Geophys. Geosyst. 17, 1–14.
Mullender, T.A.T., Velzen, A.J., Dekkers, M.J., 1993. Continuous drift correction and separate identification of ferrimagnetic and paramagnetic contributions in thermomagnetic runs. Geophys. J. Int. 114, 663–672.
Muzylev, N.G., Tabachnikova, I.P., 1987. Zonal division of lower Maikop sediments in the Caucasus and adjacent regions on the basis of nannoplankton. Sov. Geol. 1, 65–74.
Muzylöv, N.G., 1996. Early Paleogene Episodes of Eruptive Activity in the East Peri-Tethys and Their Possible Influence on the Marine Microbiota (In Russian). Foss. Microorg. As Basis Phaneroz. Stratigr. Correl. Paleobiogeography Moscow, GEOS, Vopr. Mikropaleotologii, vol. 31. pp. 128–132.
Nagymarosy, A., Voronina, A.A., 1993. Calcareous nannoplankton from the lower Maykopian beds (Early Oligocene, Union of Independent States). Knihovnicka ZPN 2, 189–223.
Ozsvárt, P., Kocsis, L., Nyerges, A., Gy, O., Pálfy, J., 2016. The eocene-oligocene climate transition in the central Paratethys. Palaeogeogr. Palaeoclimatol. Palaeoecol. 459, 471–487.
Palcu, D.V., Popov, S.V., Golovina, L.A., Kuiper, K.F., Liu, S., Krijgsman, W., 2019. The shutdown of an anoxic giant: magnetostratigraphic dating of the end of the Maikop Sea. Gondwana Res. 67, 82–100.
Passier, H.F., Dekkers, M.J., de Lange, G.J., 1998. Sediment chemistry and magnetic properties in an anomalously reducing core from the eastern Mediterranean Sea. Chem. Geol. 152, 287–306.
Perch-Nielsen, K., 1985. Mesozoic calcareous nannofossils. In: Perch-Nielsen, K. (Ed.), Plankton Stratigraphy. Cambridge University Press, pp. 329–426.
Piller, W.E., Harzhauser, M., Mandic, O., 2004. Miocene Central Paratethys stratigraphy – current status and future directions. Stratigraphy 4, 151–168.
Popov, S.V., Akhmetiev, M.A., Bugrova, E.M., Lopatin, A.V., Amitrov, O.V., Andreeva-Grigorovich, A.S., Zherikhin, V.V., Zaporozhets, N.I., Nikolaeva, I.A., Kaasheninnikov, V.A., Kuzmicheva, E.I., Sytchevskaja, E.K., Shcherba, I.G., 2001. Biogeography of the northern peri-tethys from the late Eocene to the early Miocene: Part 1. Late Eocene. Paleontol. J. 35, 1–69.
Popov, S.V., Tabachnikova, I.P., Bannikov, A.F., Sytchevskaya, E.K., Pinchuk, T.N., Akhmet'ev, M.A., Zaporozhets, N.I., van der Boon, A., Krijgsman, W., Stolyarov, A.S., Krhovsky, J., 2019a. Lectostratotype of the maikopian group in the Belaya River section upstream of the town of Maikop (western ciscaucasia) in the Oligocene part. Stratigr. Geol. Correl. 27, 339–360.
Popov, S.V., Rögl, F., Rozanov, A.Y., Steininger, F.F., Shcherba, I.G., Kovac, M., 2004a. Lithological-Paleogeographic Maps of Paratethys - 1- Maps Late Eocene to Pliocene. Courier Forschungs-Institut Senckenberg, Frankfurt am Main.
Popov, S.V., Studencka, B., 2015. Brackish-water solenovian mollusks from the lower Oligocene of the polish carpathians. Paleontol. J. 49, 342–355.
Popov, S.V., Bugrova, E.M., Amitrov, O.V., Akhmetiev, M.A., Zaporozhets, N.I., Nikolaeva, I.A., Sychevskaja, E.K., Shcherba, I.G., 2004b. Biogeography of the northern peri-tethys from the late Eocene to the early Miocene. Part 3. Late oligocene-early Miocene. Mar. Basins. Paleontol. J. 38, S653–S716.
Popov, S.V., Tabachnikova, I.P., Pinchuk, T.N., Akhmetiev, M.A., Zaporozhets, N.I., 2019b. The reference section of Eocene deposits in the Belaya River valley, Adygea, western ciscaucasia. Stratigr. Geol. Correl. 27, 118–132.
Prokopov, K.A., 1937. Essay on geological formations in the kuban river valley between sulimov and krasnogorsk. Tr. Geol. Sluz. Groznefti 8, 30–63.
Radionova, E.P., Beniamovski, V.N., Iakovleva, A.I., Muzylöv, N.G., Oreshkina, T.V., Shcherbinina, E.A., Kozlova, G.E., 2003. Early Paleogene transgressions: stratigraphical and sedimentological evidence from the northern Peri-Tethys. Geol. Soc. Am. Spec. Pap. 369, 239–261.
Rögl, F., 1998. Palaeogeographic considerations for mediterranean and Paratethys seaways (Oligocene to Miocene). Ann. Naturhistorisches Museum Wien 99, 279–310.
Rögl, F., 1999. Mediterranean and paratethys. Facts and hypotheses OF an oligocene to miocene paleogeography (short overview). Geol. Carpathica 50, 339–349.
Rowe, H., Hughes, N., Robinson, K., 2012. The quantification and application of handheld energy-dispersive x-ray fluorescence (ED-XRF) in mudrock chemostratigraphy and geochemistry. Chem. Geol. 324–325, 122–131.
Sachsenhofer, R.F., Popov, S.V., Akhmetiev, M.A., Bechtel, A., Gratzer, R., Groß, D., Horsfield, B., Rachetti, A., Rupprecht, B., Schaffar, W.B.H., Zaporozhets, N.I., 2017. The type section of the Maikop group (Oligocene–lower Miocene) at the Belaya River (North Caucasus): depositional environment and hydrocarbon potential. Am. Assoc. Petrol. Geol. Bull. 101, 289–319.
Sachsenhofer, R.F., Popov, S.V., Ćorić, Stjepan, Mayer, J., Misch, D., Morton, M.T., Pupp, M., Rauball, J., Tari, G.C., 2018. Paratethyan petroleum source rocks: an overview. J. Pet. Geol. 41, 219–245.
Sachsenhofer, R.F., Schulz, H.-M., 2006. Architecture of Lower Oligocene source rocks in the Alpine Foreland Basin: a model for syn- and post-depositional source-rock features in the Paratethyan realm. Pet. Geosci. 12, 363–377.
Sahy, D., Condon, D.J., Hilgen, F.J., Kuiper, K.F., 2017. Reducing disparity in radio-isotopic and astrochronology-based time scales of the late Eocene and Oligocene. Paleoceanography 32, 1018–1035.
Saint-Germes, M.L., Bazhenova, O.K., Baudin, F., Zaporozhets, N.I., Fadeeva, N.P., 2000. Organic matter in Oligocene Maikop sequence of the north Caucasus. Lithol. Miner. Resour. 35, 47–62.
Schulz, H., Bechtel, A., Sachsenhofer, R.F., 2005. The birth of the Paratethys during the early Oligocene: from tethys to an ancient Black Sea analogue? Glob. Planet. Chang. 49, 163–176.
Seiter, K., Hensen, C., Schröter, J., Zabel, M., 2004. Organic carbon content in surface sediments — defining regional provinces. Deep. Res. I 51, 2001–2026.
Shcherbinina, E., Gavrilov, Y., 2007. Paleogene oxygen depletion episodes in the northeastern Peri-Tethys: a regional response to global events. In: Geophysical Research Abstracts.
Sluijs, A., Zeebe, R.E., Bijl, P.K., Bohaty, S.M., 2013. A middle Eocene carbon cycle

conundrum. Nat. Geosci. 6, 429–434.
Stephenson, A., 1993. Three-Axis static alternating field demagnetization of rocks and the identification of natural remanent magnetization, gyroremanent maghetization, and anisotropy. J. Geophys. Res. 98, 373–381.
Stolyarov, A.S., 1993. About genesis of the largest Phanerozoic sedimentary concentrations of manganese and the forecast of their genetic analogues in Russia. Father. Geol. 5, 28–33 in Russ.
Tauxe, L., Kent, D., 2004. A simplified statistical model for the geomagnetic field and the detection of shallow bias in paleomagnetic inclinations: Was the ancient magnetic field dipolar. Timescales of the Paleomagnetic Field 145, 101–115. https://doi.org/10.1029/145GM08.
Tauxe, L., Kodama, K., Kent, D.V., 2008. Testing corrections for paleomagnetic inclination error in sedimentary rocks: a comparative approach. Phys. Earth Planet. Inter. 169, 152–165.
Torsvik, T.H., Van der Voo, R., Preeden, U., Niocaill, C.Mac, Steinberger, B., Doubrovine, P.V., van Hinsbergen, D.J.J., Domeier, M., Gaina, C., Tohver, E., Meert, J.G., McCausland, P.J.A., Cocks, L.R.M., 2012. Phanerozoic polar wander, palaeogeography and dynamics. Earth Sci. Rev. 114, 325–368.
Tribovillard, N., Algeo, T.J., Lyons, T., Riboulleau, A., 2006. Trace metals as paleoredox and paleoproductivity proxies: an update. Chem. Geol. 232, 12–32.
van der Boon, A., Beniest, A., Ciurej, A., Gaździcka, E., Grothe, A., Sachsenhofer, R.F., Langereis, C.G., Krijgsman, W., 2018. The eocene-oligocene transition in the north alpine foreland basin and subsequent closure of a Paratethys gateway. Glob. Planet. Chang. 162, 101–119.
Vandenberghe, N., Hilgen, F.J., Speijer, R.P., Ogg, J.G., Gradstein, F.M., Hammer, O., Hollis, C.J., Hooker, J.J., 2012. The Geologic Time Scale: the Paleogene Period, the Geologic Time Scale. Elsevier.
Varentsov, I.M., 2002. Genesis of the Eastern Paratethys manganese ore giants: impact of events at the Eocene/Oligocene boundary. Ore Geol. Rev. 20, 65–82.
Varentsov, I.M., Muzyliov, N.G., Nikolaev, V.G., Stupin, S.I., 2003. The origin of black shale-hosted Mn deposits in Paratethyan basins: constraints from geological events at the Eocene/Oligocene boundary. Russ. J. Earth Sci. 5, 255–272.
Verdel, C., Wernicke, B.P., Hassanzadeh, J., Guest, B., 2011. A Paleogene extensional arc flare-up in Iran. Tectonics 30.
Vermeesch, P., 2012. On the visualisation of detrital age distributions. Chem. Geol. 312–313, 190–194.
Veto, I., 1987. An Oligocene sink for organic carbon: upwelling in the Paratethys? Palaeogeogr. Palaeoclimatol. Palaeoecol. 60, 143–153.
Zakrevskaya, E., Beniamovsky, V., Less, G., Báldi-beke, M., 2011. Integrated biostratigraphy of Eocene deposits in the gubs section (northern Caucasus) with special attention to the ypresian/lutetian boundary and to the peritethyan- tethyan correlation. Turk. J. Earth Sci. 20, 753–792.
Zijderveld, J.D.A., 1967. AC demagnetization of rocks: analysis of results. In: Collinson, D.W., Creer, K.M. (Eds.), Methods in Paleomagnetism. Elsevier, Amsterdam, pp. 254–286.